Institute for Communications and Navigation

Heading Estimation with Novatel's low cost OEMStar Receiver

Carl Felix Hammes

Supervised by Dr.-Ing. Patrick Henkel

Dezember 03, 2012

Institute for Communications and Navigation
Univ.-Prof. Dr. sc. nat. Christoph Günther

Technische Universität München
Theresienstrasse 90
80333 Munich

Submitted for the degree *Bachelor of Science*
at the faculty *Elektrotechnik und Informationstechnik*
at *Technische Universität München (TUM)*

Email: felixhammes@mytum.de

Layout by LaTeX 2_ε

Abstract

Precise attitude determination with Global Navigation Satellite System (GNSS) is interesting for many applications e.g. space, air, ship and car navigation. But it is only possible if one is capable to resolve the integer ambiguity of the carrier phase measurement. This bachelor thesis addresses on the one hand the requirements for double difference integer ambiguity resolution to a receiver design and analyzes if the NovatelOEMStar™receiver fulfills the requirements. On the other hand this thesis shows that heading estimation with an accuracy of 0.02° is feasible. As addition a soft constrained ambiguity resolution algorithm is discussed and an idea how this algorithm could be improved is developed.

Contents

1. Introduction **4**

2. Measurement Model **8**
2.1 Standard GPS Observation Equation 8
2.2 Advanced GPS Carrier-Phase Observation Equation 9
2.2.1 Case 1: Base Band 12
2.2.2 Case 2: Intermediate Frequency 13
2.3 Difference GNSS Models 15
2.3.1 Single Difference 15
2.3.2 Double Difference 15
2.4 Summary: Receiver Requirements for Double Difference Integer Ambiguity Resolution 16
2.5 General linear(ized) GNSS Model formulation 17
2.5.1 Single Epoch Model with only Carrier phase Measurement 17
2.5.2 Single Epoch Model with Code and Carrier-Phase Measurement 18
2.5.3 Multi Epoch Model with Code and/or Carrier-Phase Measurement 18

3. Ambiguity Resolution Algorithms **19**
3.1 Standard Integer Least Squares Problem 19
3.2 Soft Constrained Ambiguity Resolution - Spherical A Priori Knowledge 21
3.2.1 Maximum A Posteriori Probability Estimator 21
3.2.2 Constrained Integer Search 23
3.3 Soft Constrained Ambiguity Resolution - Position Domain A Priori Knowledge . 27
3.3.1 Maximum A Posteriori Probability Estimator 27
3.3.2 Constrained Integer Search 29

4. Experimental Results **33**
4.1 Receiver Setup 33
4.1.1 Novatel OEMStar™Receiver 33
4.1.2 Laptop and Control Software 33
4.1.3 Antennas 34
4.1.4 Coaxial Cable 34
4.2 Receiver Quality Analysis 35
4.2.1 Zero Baseline Test 35
4.2.2 Receiver Clock Errors 38
4.3 Stationary Measurement 40
4.3.1 Measurement Setup 40
4.3.2 Measurement Results 40
4.4 Maritime Application 44
4.4.1 Measurement Setup 44

4.4.2 Measurement Results 44

5. Conclusion **49**

Appendix **50**
A1. Cholesky Decomposition 50
A2. Chi-Squared Distribution 51
A3. Acronyms 52

Bibliography **55**

1. Introduction

During the last decades the evolving Global Navigation Satellite Systems (GNSSs) changed the field of positioning and navigation in a tremendous way. The signals serve much more applications than intended in the early times of their development. One of those is to use multiple-antennas with a rigid structure fixed to a moving object to determine the attitude. A configuration with three antennas could be used for full attitude determination. Explicitly speaking all three rotation angels between a body-fixed coordinate frame and the local East-North-Up Coordinate Frame (ENU) can be determined. In this thesis the focus is on maritime applications like guiding ships through narrow-water gates, for the approach of a port or just to maintain the correct course on water ways with a high volume of traffic. For those applications full attitude determination is not required because there is no need to determine the rotation around the longitudinal axis of a ship. Therefore attitude determination for ships could be performed with two antennas. An example could be seen in figure 1.1

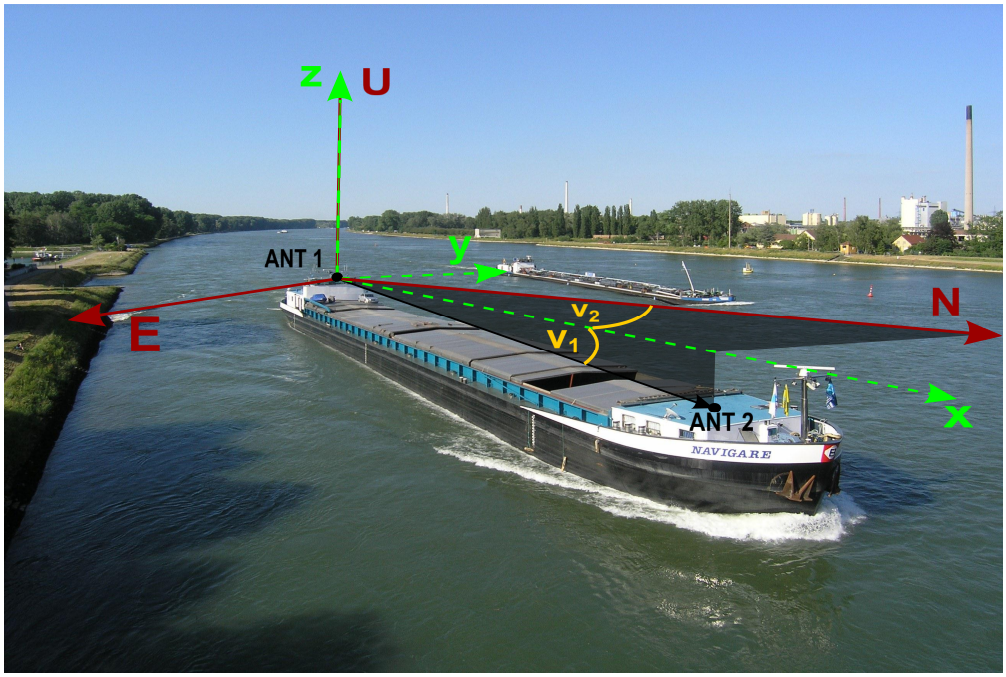

Figure 1.1: Two inland water vessels navigating close to each other on a water way. By Ikar.us (Karlsruhe:Bild:SchiffeMaxau.jpg) [CC-BY-2.0-de (http://creativecommons.org/licenses/by/2.0/de/deed.en)], via Wikimedia Commons

For that type of application usually antenna separations of 2-500m are common. In this thesis we call that a short baseline as atmospheric delays are suppressed over these baseline length. To determine the attitude in such configurations, with an angular accuracy of 0.02°, the baseline error for a 20m baseline has to be less than 6mm, due to its dependance on the baseline lengths. GNSSs allow measurement of the code and the carrier phase. The noise of the carrier phase measurement is in the order of one to two millimeters which is two to three orders of magnitude lower than the

noise of the code measurement. It is obvious that only carrier phase measurements could meet the accuracy requirements for this type of application. The carrier phase measurement is obtained in a Phase Look Loop (PLL), which tracks the phase of the carrier signal by comparing the phase of the receiver generated replicas to the carrier phase of the signal received from the satellites. Due to the periodicity of the carrier signal, this measurement has an ambiguity in the number of whole cycles. For that reason it is only an indirect measurement of the range between the receiver and the satellite. Figure 1.2 shows the possible locations of the antenna besides the true location. The separation of the lines is the wavelength of the carrier frequency. For this thesis only measurements of the L1 signal of the Global Positioning System (GPS) were used with a wavelength of 19cm. One can see that we could gain heading information with the required accuracy only from the carrier phase measurement if we can resolve the integer ambiguities correctly. The key to high-precision is to resolve the unknown cycle ambiguity. Only for the sake of completeness it should be mentioned that the reliability of the ambiguity resolution process could be dramatically improved by using multi-frequency combinations which increase the effective wavelength and reduce ionospheric delays [1]. Due to the case that only GPS L1 single-frequency measurements are used in this thesis this technique could not be applied.

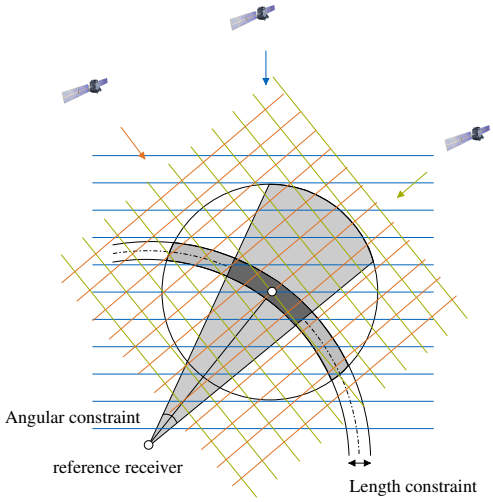

Figure 1.2: Integer Ambiguity

Like Peter Buist in [2] we will summarize and group the different approaches to resolve the carrier phase ambiguities. Figure 1.3 gives you an overview.

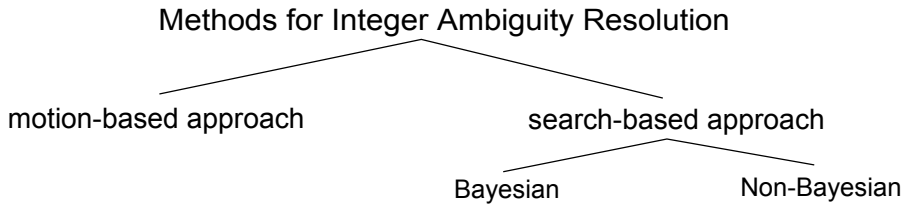

Figure 1.3: Classification of integer ambiguity resolution techniques.

First Buist distinguished between the earlier motion-based approaches and the search-based approaches. The older motion-based methods require a change in the receiver-satellite geometry e.g. the receiver changes its position or attitude or the satellite travels further. These methods have

the major disadvantage that they need by definition a minimum time period and sometimes even a rough knowledge of the initial attitude. Secondly, there are the search-based approaches, which include all state of the art methods to resolve the integer ambiguities. These methods are further distinguished by Buist in Bayesian and non-Bayesian approaches. Thus it had been done by Verhagen and Teunissen in [3] before. Non-Bayesian approaches take only the observation as random variables into account. They could be formulated e.g. as Maximum Likelihood (ML) estimator, which maximizes the probability for the measurement generated by the unknown parameters. The widely used Least Squares Ambiguity Decorrelation Adjustment (LAMBDA) method belongs to this group. This method was introduced by Teunissen in [4]. The LAMBDA method performs the search for the best integer in a transformed space, in which the integer ambiguities are decorrelated from each other. This transformation increases the efficiency of the search dramatically. The decorrelation transformation is therefore also used in other algorithms which implement the search in a different way.
In cases like attitude determination prior information could be used to either validate the solution gained by an unconstrained method or to use the information directly during the process of estimation which leads to the constrained methods. The Bayesian approaches consider in addition to the observations, the unknown baseline and ambiguity parameters as random variables. With assumptions on the probability distribution they search for the most likely solution. In [5] the LAMBDA method is expanded to the Multivariate Constrained - LAMBDA (MC-LAMBDA) method. That algorithm uses the constraint to adjust the size of the search space in an intelligent way to both maximize the success rate as well as to minimize the computation time. The prior mentioned method can be considered as a tight constrained, due to the fact that the algorithm accounts for the constrained parameters, like the baseline length, as exact values. Henkel and Jurkowski have developed in [6][7] a Maximum A Posteriori Probability (MAP) estimation method for soft constrained ambiguity resolution for applications where the baseline and its length is not known with sufficient accuracy. The knowledge of the baseline length as well as the pitch and heading angles are assumed to have a certain probability distribution e.g. Gaussian. A possible reason is the antenna phase center offset, which could be as large as 15cm for low-cost L1 antennas and thereby, is in the same order of magnitude as the wavelength. A second reason is the torsion of ships or aircraft wings which can lead to substantial variations in the baseline.
As an first step of this thesis the performance of the NovaltelOEMStar™receiver for integer ambiguity resolution with double difference measurements should be analyzed. The NavatelOEMStar™receiver is the cheapest single frequency receiver of this manufacturer. Therefore the receiver requirements for integer-valued ambiguities are provided. As the main objective the data of the Precise and integer Localisation and Navigation in Rail and Inlandwater Traffic (PiLoNav) measurement campaign should be analyzed. With ambiguity resolution methods it should be shown that heading angle, pitch angle and baseline length estimation is possible with very high accuracies. Chapter 2 introduces the underlying model and notations used throughout the thesis. Further a more detailed view on the carrier phase measurement is done to derive the tracking requirements for integer valued ambiguities. At last the formulation and advantages of single and double difference measurements are mentioned. Chapter 3 deals with the theoretical description of the soft constrained ambiguity resolution algorithms. At the beginning the unconstrained Integer Least Squares (ILS) estimator with the orthogonal decomposition is introduced. Further the soft constrained ambiguity resolution algorithm is explained. Then as an addition a new idea is introduced how the current soft constrained ambiguity resolution algorithm could be improved. Chapter 4 begins with a description of the used equipment during the different measurements.

Subsequently the results of the receiver quality analysis are shown. After that the setup for the stationary and maritime measurements are explained and the results will be discussed. This section shows which highly accurate results could be obtained with the Novatel OEMStar™receiver by correct resolved integer ambiguities. Chapter 5 concludes the work performed and outlines future questions.

2. Measurement Model

2.1 Standard GPS Observation Equation

Global Navigation Satellite System (GNSS) receivers use a Delay Locked Loop (DLL) and a Phase Look Loop (PLL) to track the pseudoranges and the carrier phases. As in [8][9][10] the pseudoranges ρ_r^k and the carrier phase $\lambda\phi_r^k$ of receiver r and satellite k are modeled like this:

$$\rho_r^k = r_r^k + c(\delta\tau_r - \delta\tau^k) + I_r^k + T_r^k + \eta_r^k \tag{2.1}$$

$$\lambda\phi_r^k = r_r^k + c(\delta\tau_r - \delta\tau^k) - I_r^k + T_r^k + \lambda N_r^k + \varepsilon_r^k \tag{2.2}$$

The first equation (2.1) is the general model for the measurement obtained from the delay of the spread spectrum code of the Code Division Multiple Access (CDMA) signal from satellite k received at receiver r. The second and for this thesis more important equation (2.2) models the measurement of the carrier phase. In contrast to the equation (2.1) the carrier phase measurement is ambiguous, resulting in the carrier phase ambiguity λN_r^k . The following notations apply:

ρ_r^k	pseudorange between receiver r and satellite k
ϕ_r^k	carrier phase measured between receiver r and satellite k
r_r^k	true geometrical distance between receiver r and satellite k defined as $r_r^k = \|\vec{x}_r - \vec{x}^k\|$
$\delta\tau_r$	clock offset of receiver r
$\delta\tau^k$	clock offset of satellite k
I_r^k	ionospheric delay
T_r^k	tropospheric delay
N_r^k	carrier phase integer ambiguity
η_r^k	pseudorange noise including other unmodeled effects like multipath
ϵ_r^k	phase noise including other unmodeled effects
λ	carrier wavelength (L1)
c	speed of light

The equations above are nonlinear with respect to the user position $\vec{\boldsymbol{x}}_r$, but can be well-linearized using the unit vector $\vec{\boldsymbol{e}}_r^k$ pointing from the satellite k to the receiver r,i.e.

$$r_r^k = (\vec{\boldsymbol{e}}_r^k)^T(\vec{\boldsymbol{x}}_r - \vec{\boldsymbol{x}}^k) \quad \text{with} \quad \vec{\boldsymbol{e}}_r^k = \frac{\vec{\boldsymbol{x}}_r - \vec{\boldsymbol{x}}^k}{\|\vec{\boldsymbol{x}}_r - \vec{\boldsymbol{x}}^k\|} \tag{2.3}$$

Consequently, (2.1) and (2.2) can be rewritten as:

$$\rho_r^k = (\vec{\boldsymbol{e}}_r^k)^T(\vec{\boldsymbol{x}}_r - \vec{\boldsymbol{x}}^k) + c(\delta\tau_r - \delta\tau^k) + I_r^k + T_r^k + \eta_r^k \tag{2.4}$$

$$\lambda\phi_r^k = (\vec{\boldsymbol{e}}_r^k)^T(\vec{\boldsymbol{x}}_r - \vec{\boldsymbol{x}}^k) + c(\delta\tau_r - \delta\tau^k) - I_r^k + T_r^k + \lambda N_r^k + \epsilon_r^k \tag{2.5}$$

2.2 Advanced GPS Carrier-Phase Observation Equation

The aim of this subsection is to clarify, from a theoretical perspective, if the basic GNSS carrier phase measurement model is adequate for the application addressed in this thesis. That means explicitly, under which conditions will it be possible to resolve the carrier phase ambiguity as integers. By having a closer look, how a carrier phase measurement is obtained in a GNSS receiver, it will be shown that some requirements to the receiver construction apply to be applicable for integer ambiguity resolution. Because we are interested only in the influences of the receiver structure on the carrier phase measurement, this model is reduced to a pure transition of a single carrier frequency without modulation. We can do this if we assume that prior to the PLL of the receiver, the demodulation of the navigation message has been performed.The PLL could use the knowledge which information bit $b = \{0, 1\}$ has been transmitted, to correct the carrier phase measurement with a $90°$ phase shift if a 0, which is modulated as -1, has been transmitted. That is our first requirement to the receiver, otherwise not only full cycle integer ambiguities are possible, although ambiguities with half cycles occur.

1st Requirement: The receiver detects and corrects phase jumps of $\delta\phi = \pm 0.5$ cycles due to the modulated navigation message.

With respect to Cillian O'Driscoll's explanations in [11] the following model is considered. The notation for the timescale is defined as follows. All times given with respect to the internal satellite clock of the kth satellite will be mentioned with $\hat{t}^k$, with respect to the internal receiver clock as $\check{t}_r$ and in GPS system time scale as t. For the definition of the different time events see figure 2.1.

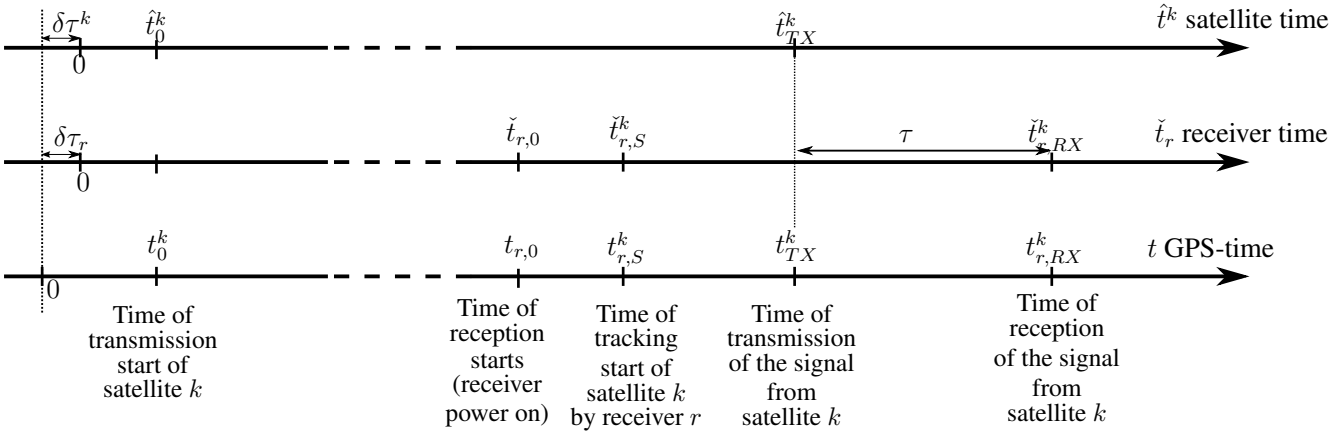

Figure 2.1: Time scale definition

The different time scale could be related to each other by $t := \hat{t}^k - \delta\tau^k$ for the satellite and Global Positioning System (GPS) timescale and by $t := \check{t}_r - \delta\tau_r$ for the receiver and the GPS timescale. To simplify the description, this model assumes ideal oscillators in the satellite and the receiver, but bearing in mind that this would also mean constant satellite and receiver clock offsets, which is not true. With this assumption the integration of frequency in the course of time to obtain the carrier phase, can be written in the following way:

$$\phi(t) = \phi(t_0) + \int_{t_0}^{t} f(s)\, ds = \phi(t_0) + f \cdot (t - t_0) \tag{2.6}$$

The satellite k transmits a sinusoidal carrier wave at frequency L1 with a certain phase in relation to its own clock, denoted as $\phi^k_{RF}(\hat{t}^k_{TX})$. The receiver r receives the transmitted sinusoidal carrier wave at its position τ seconds later, at the time of reception according to the receiver clock $\check{t}^k_r = \check{t}^k_{TX} + \tau$, denoted as $\phi^k_{r,RF}(\check{t}^k_{r,RX})$. During the transmission time from the satellite to the receiver the carrier signal undergoes a phase advance by the Ionosphere I^k_r and a delay by the Troposphere T^k_r. Figure 2.2 shows that setup.

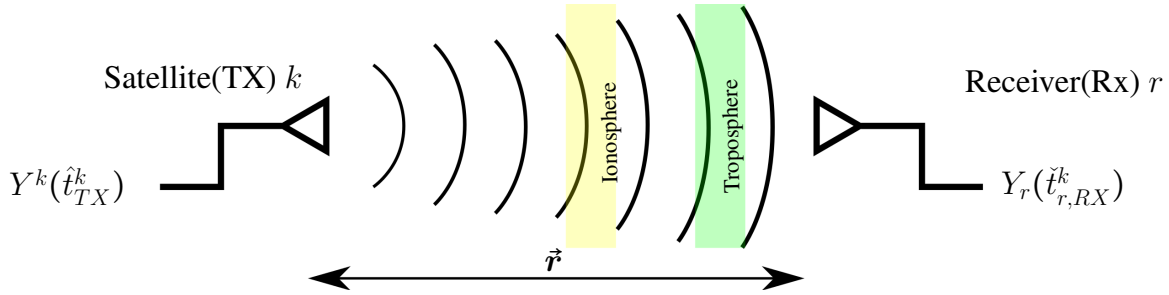

Figure 2.2: Propagation Model for Carrier Phase Measurement

The transmitted and received signals could be described as follows:

$$Y^k(\hat{t}^k_{TX}) = A^k(\hat{t}^k_{TX}) \exp\left(j2\pi\phi^k_{RF}(\hat{t}^k_{TX})\right) \quad \phi^k_{RF}(\hat{t}^k_{TX}) = f_{RF}\hat{t}^k_{TX} + \phi^k_0 \quad \phi^k_0 := \phi^k_{RF}(\hat{t}^k_0) \tag{2.7}$$

$$Y_r(\check{t}^k_{r,RX}) = A_r(\check{t}^k_{r,RX}) \exp\left(j2\pi\phi^k_{r,RF}(\check{t}^k_{r,RX})\right) \tag{2.8}$$

With the model described above one could derive the description of the received carrier phase at the receiver r by taking into account that the phase received at the reception time $\phi^k_{r,RF}(\check{t}^k_{r,RX})$ is the same as the phase at the satellite at the transmission time instance $\phi^k_{RF}(\hat{t}^k_{TX})$. In the atmospheric free case the received phase could be derived as an integration of the frequency over the travel time interval. With ionospheric phase advance and tropospheric delays we have to account for this effects. Therefore the following equation is true:

$$\phi^k_{RF}(\hat{t}^k_{RX}) = \phi^k_{RF}(\hat{t}^k_{TX}) + f_{RF} \cdot \tau = \phi^k_{RF}(\hat{t}^k_{TX}) + \frac{I^k_r}{\lambda} - \frac{T^k_r}{\lambda} + \frac{r^k_r(\check{t}^k_{r,RX})}{\lambda} \tag{2.9}$$

With (2.9) and the definition of the phase of the satellite at transmission time from (2.7) it is easy to derive (2.11).

$$\phi^k_{r,RF}(\check{t}^k_{r,RX}) = \phi^k_{RF}(\hat{t}^k_{TX}) \tag{2.10}$$

$$\begin{aligned}
\phi^k_{r,RF}(\check{t}^k_{r,RX}) &= \phi^k_{RF}(\hat{t}^k_{RX}) + \frac{I^k_r}{\lambda} - \frac{T^k_r}{\lambda} - \frac{r^k_r(\check{t}^k_{r,RX})}{\lambda} \\
\phi^k_{r,RF}(\check{t}^k_{r,RX}) &= f_{RF}\hat{t}^k_{RX} + \phi^k_0 + \frac{I^k_r}{\lambda} - \frac{T^k_r}{\lambda} - \frac{r^k_r(\check{t}^k_{r,RX})}{\lambda} \\
\phi^k_{r,RF}(\check{t}^k_{r,RX}) &= f_{RF}\check{t}^k_{RX} + \phi^k_0 + f_{RF}(\delta\tau^k - \delta\tau_r) + \frac{I^k_r}{\lambda} - \frac{T^k_r}{\lambda} - \frac{r^k_r(\check{t}^k_{r,RX})}{\lambda}
\end{aligned} \tag{2.11}$$

In equation (2.11) we have got a formulation which describes the received phase at the antenna of the receiver r. In Figure 2.3 we see the further steps how a model receiver processes the signals.

After bandpass filtering the signal is down converted to an Intermediate Frequency (IF) or to the base band. This mixing process simplifies the signal processing but may affect the carrier phase

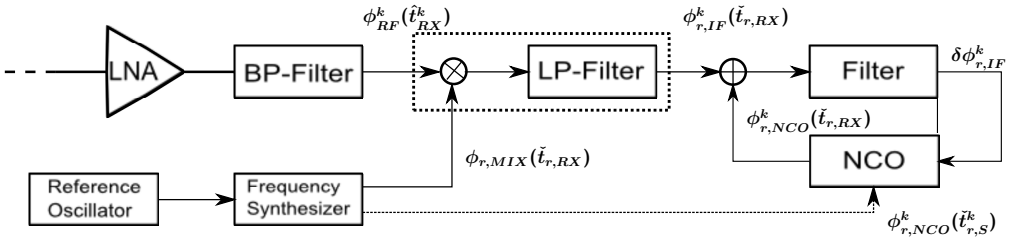

Figure 2.3: Simple Model for Carrier Phase Measurement

measurement if not designed well. The mixing is mainly a multiplication of the received signal with a receiver generated signal at a certain frequency, designed according to the frequency plan of the receiver. With the low pass filter after the multiplication the output signal is at the desired IF.

$$Y_{r,MIX}(\check{t}_{r,RX}) = A_{r,MIX}(\check{t}_{r,RX}) \exp\left(j2\pi\phi_{r,MIX}(\check{t}_{r,RX})\right) \tag{2.12}$$

$$\phi_{r,MIX}(\check{t}_{r,RX}) = (f_{RF} - f_{IF})\check{t}_{r,RX} + \phi_{r,MIX0} \qquad \phi_{r,MIX0} := \phi_{r,MIX}(\check{t}_{r,0}) \tag{2.13}$$

The effect of the mixing process is in relation to the phase of the signal just a subtraction of the phases as seen in (2.14). With that one could formulate the phase of the intermediate frequency in the next step:

$$\phi^k_{r,IF}(\check{t}_{r,RX}) = \phi^k_{r,RF}(\check{t}_{r,RX}) - \phi_{r,MIX}(\check{t}_{r,RX}) \tag{2.14}$$

$$\begin{aligned}\phi^k_{r,IF}(\check{t}_{r,RX}) =& f_{RF}\check{t}^k_{RX} + \phi^k_0 + f_{RF}(\delta\tau^k - \delta\tau_r) + \frac{I^k_r}{\lambda} - \frac{T^k_r}{\lambda} - \frac{r^k_r(\check{t}^k_{r,RX})}{\lambda} \\ & - (f_{RF} - f_{IF})\check{t}_{r,RX} + \phi_{r,MIX0} \\ \phi^k_{r,IF}(\check{t}_{r,RX}) =& f_{IF}\check{t}_{r,RX} - \phi_{r,MIX0} + \phi^k_0 + f_{RF}(\delta\tau^k - \delta\tau_r) + \frac{I^k_r}{\lambda} - \frac{T^k_r}{\lambda} - \frac{r^k_r(\check{t}^k_{r,RX})}{\lambda}\end{aligned} \tag{2.15}$$

When the signal is at the IF, in a modern receiver the signal will be sampled and with an Analog Digital Converter (ADC) digitized. The further processing is then performed with digital signal processors. In our simplified model the next step is the PLL, noting that for real GNSS receivers, parallel for each tracking channel the spread-spectrum-code has to be removed by a correlation process before the tracking loops can acquire the signal of satellite k. The PLL drives the phase difference $\delta\phi^k_{r,IF}$ to zero by steering the Numerical Controlled Oscillator (NCO). For this process you have to take into account that the NCO has to be initialized with a certain phase $\phi^k_{r,NCO}(\check{t}^k_{r,S})$ at the time a new satellite signal is received. We will see later that this initialization is a crucial aspect for integer ambiguity resolution. With the denoted structure the PLL knows the fractional part of the carrier phase at the input $\phi^k_{r,IF}(\check{t}_{r,RX})$, mathematically defined in (2.16). The noise term $\tilde{\varepsilon}^k_r$ is introduced at that stage to denote the carrier phase measurement noise.

$$\phi^k_{r,NCO}(\check{t}_{r,RX}) = \left[\phi^k_{r,IF}(\check{t}_{r,RX})\right] \bmod 1 + \tilde{\varepsilon}^k_r \tag{2.16}$$

Further the receiver should integrate the NCO phase $\phi^k_{r,NCO}(\check{t}_{r,RX})$ and store the number of full cycles of its generated reference signal defined as the integer component of the NCO phase $L^k_r(\check{t}_{r,RX})$. If the first requirement is fulfilled the integer component of the NCO phase increases and decreases as the unknown integer component we are interested in.

2nd Requirement: The PLL of the receiver should integrate the NCO phase $\phi^k_{r,NCO}(\check{t}^k_{r,RX})$ and store the number of full cycles of its generated reference signal defined as the integer component of the NCO phase, noted as $L^k_r(\check{t}^k_{r,RX})$.

In the following section the internal generation of the carrier phase measurement is described for two different frequency plans. Starting with the simpler case in which the signal is down converted to the base band followed by the case in which the signal is transferred to a IF greater than zero.

2.2.1 Case 1: Base Band

For the first case we consider an IF defined as zero ($f_{r,IF} = 0$). That leads to a simplification of the phase after the mixing process in the base band. Due to consistency with figure 2.3 we keep the index IF. The first term in equation (2.15) drops out and we get (2.17) for the phase tracked by the PLL:

$$\phi^k_{r,IF}(\check{t}_{r,RX}) = -\phi_{r,MIX0} + \phi^k_0 + f_{RF}(\delta\tau^k - \delta\tau_r) + \frac{I^k_r}{\lambda} - \frac{T^k_r}{\lambda} - \frac{r^k_r(\check{t}^k_{r,RX})}{\lambda} \tag{2.17}$$

Now the question arises: How do we generate a useful measurement of the carrier phase representing mainly the range between the receiver and the satellite $r^k_r(\check{t}^k_{r,RX})$. In this case we define the negative of the fractional part of the NCO phase plus the stored full cycle integer component, as our measurement. We will see why this is a reasonable choice.

$$\tilde{\phi}^k_r(\check{t}_{r,RX}) := -\phi^k_{r,NCO}(\check{t}_{r,RX}) + L^k_r(\check{t}_{r,RX}) \tag{2.18}$$

With this definition we can derive the observation equation for the carrier phase with the prior derived expressions. In the third equation the modulo operator is removed by introducing the number of unknown full cycle integers between the satellite and the receiver denoted as $K^k_r(\check{t}_{r,RX})$. In the fourth step the well-known integer ambiguity is introduced as N^k_r. It is the difference between the known integer component of the NCO phase and the unknown integer component of the received signal.

$$\begin{aligned}
\tilde{\phi}^k_r(\check{t}_{r,RX}) &= -\left[\phi^k_{r,IF}(\check{t}_{r,RX})\right] \bmod 1 + L^k_r(\check{t}_{r,RX}) + \tilde{\varepsilon}^k_r \\
\tilde{\phi}^k_r(\check{t}_{r,RX}) &= -\left[-\phi_{r,MIX0} + \phi^k_0 + f_{RF}(\delta\tau^k - \delta\tau_r) + \frac{I^k_r}{\lambda} - \frac{T^k_r}{\lambda} - \frac{r^k_r(\check{t}^k_{r,RX})}{\lambda} \right] \bmod 1 + L^k_r(\check{t}_{r,RX}) + \tilde{\varepsilon}^k_r \\
\tilde{\phi}^k_r(\check{t}_{r,RX}) &= -\left[-\phi_{r,MIX0} + \phi^k_0 + f_{RF}(\delta\tau^k - \delta\tau_r) + \frac{I^k_r}{\lambda} - \frac{T^k_r}{\lambda} - \frac{r^k_r(\check{t}^k_{r,RX})}{\lambda} + K^k_r(\check{t}_{r,RX}) \right] + L^k_r(\check{t}_{r,RX}) + \tilde{\varepsilon}^k_r \\
\tilde{\phi}^k_r(\check{t}_{r,RX}) &= \frac{r^k_r(\check{t}^k_{r,RX})}{\lambda} - f_{RF}(\delta\tau^k - \delta\tau_r) - \frac{I^k_r}{\lambda} + \frac{T^k_r}{\lambda} + \phi_{r,MIX0} - \phi^k_0 + \underbrace{(L^k_r(\check{t}_{r,RX}) - K^k_r(\check{t}_{r,RX}))}_{N^k_r} + \tilde{\varepsilon}^k_r \\
\tilde{\phi}^k_r(\check{t}_{r,RX}) &= \frac{r^k_r(\check{t}^k_{r,RX})}{\lambda} + f_{RF}(\delta\tau_r - \delta\tau^k) - \frac{I^k_r}{\lambda} + \frac{T^k_r}{\lambda} + \phi_{r,MIX0} - \phi^k_0 + N^k_r + \tilde{\varepsilon}^k_r
\end{aligned} \tag{2.19}$$

Note that we explicitly dropped the time dependency for the integer ambiguity $N^k_r := L^k_r(\check{t}_{r,RX}) - K^k_r(\check{t}_{r,RX})$ because if phase look is achieved $L^k_r(\check{t}_{r,RX})$ and $K^k_r(\check{t}_{r,RX})$ should increase or decrease with the same number of integers, for that reason the difference stays constant. That is the goal of our 2nd requirement. By multiplication with lambda and a redefinition of the noise term as

$\varepsilon_r^k := \lambda \cdot \tilde{\varepsilon}_r^k$ we end in the observation equation for case 1.

$$\lambda\tilde{\phi}_r^k(\check{t}_{r,RX}) = r_r^k(\check{t}_{r,RX}^k) + c(\delta\tau_r - \delta\tau^k) - I_r^k + T_r^k + \underbrace{\lambda(\phi_{r,MIX0} - \phi_0^k)}_{\text{receiver and satellite biases}} + \lambda N_r^k + \varepsilon_r^k \tag{2.20}$$

The model shows that in the base band case biases depend either on the receiver or on the satellite. No biases depending on the receiver and the satellite are introduced. Besides that by simply chosing $\phi_{r,MIX0} = 0$ the receiver dependent bias drops out. The remaining satellite phase offset is easily removed by differencing between two receivers as later seen in subsection 2.3.

2.2.2 Case 2: Intermediate Frequency

For the second case we consider an IF defined as $f_{r,IF} > 0$. That leads to no simplification of the phase after the mixing process equation (2.15) stays the same. It contains of two time varying components besides the biases. One due to the range which we are interested in and one due to the IF which contains no information. For that reason we like to compensate for the effect of the IF on our measurement. The best case would be a measurement defined like this:

$$\tilde{\phi}_r^k(\check{t}_{r,RX}) := f_{IF}t_{r,RX}^k - \phi_{r,NCO}^k(\check{t}_{r,RX}) + L_r^k(\check{t}_{r,RX}) \tag{2.21}$$

At first sight there seems to be no problem with this definition. But bearing in mind that the term $f_{IF}t_{r,rx}^k$ is a simplification of an integration over the IF from minus infinity to the reception time $t_{r,rx}^k$ with a non-ideal oscillator in reality. Such an implementation is not feasible. Simply speaking that definition is not feasible. However to come along with that problem one implements the following measurement definition:

$$\tilde{\phi}_r^k(\check{t}_{r,RX}) := f_{IF}(\check{t}_{r,RX}^k - \check{t}_{r,S}^k) + \phi_{r,NCO}^k(\check{t}_{r,S}^k) - \phi_{r,NCO}^k(\check{t}_{r,RX}) + L_r^k(\check{t}_{r,RX}) \tag{2.22}$$

This definition can be implemented, because the first two terms form a reference signal generated on the IF with a initialization phase at time of satellite acquisition. As in case 1 we derive the observation equation for this case now. The steps are nearly the same as for case 1 by using (2.15) and (2.16) with definition (2.22):

$$\tilde{\phi}_r^k(\check{t}_{r,RX}) = f_{IF}(\check{t}_{r,RX}^k - \check{t}_{r,S}^k) + \phi_{r,NCO}^k(\check{t}^{k_r,S}) - \phi_{r,NCO}^k(\check{t}_{r,RX}) + L_r^k(\check{t}_{r,RX}) \tag{2.23}$$

$$\tilde{\phi}_r^k(\check{t}_{r,RX}) = f_{IF}(\check{t}_{r,RX}^k - \check{t}_{r,S}^k) + \phi_{r,NCO}^k(\check{t}^{k_r,S}) - [\phi_{r,IF}^k(\check{t}_{r,RX})] \mod 1 + L_r^k(\check{t}_{r,RX}) + \tilde{\varepsilon}_r^k$$

$$\begin{aligned}\tilde{\phi}_r^k(\check{t}_{r,RX}) =& \frac{r_r^k(\check{t}_{r,RX}^k)}{\lambda} - f_{RF}(\delta\tau^k - \delta\tau_r) - \frac{I_r^k}{\lambda} + \frac{T_r^k}{\lambda} \\ &+ \phi_{r,MIX0} - \phi_0^k + f_{IF}\check{t}_{r,S}^k + \phi_{r,NCO}^k(\check{t}^{k_r,S}) + \underbrace{(L_r^k(\check{t}_{r,RX}) - K_r^k(\check{t}_{r,RX}))}_{N_r^k} + \tilde{\varepsilon}_r^k\end{aligned} \tag{2.24}$$

By multiplication with lambda and a new definition of the noise term as $\varepsilon_r^k := \lambda \cdot \tilde{\varepsilon}_r^k$, we end in the observation equation for case 2.

$$\begin{aligned}\lambda\tilde{\phi}_r^k(\check{t}_{r,RX}) =& r_r^k(\check{t}_{r,RX}^k) + c(\delta\tau_r - \delta\tau^k) - I_r^k + T_r^k \\ &+ \underbrace{\lambda(\phi_{r,MIX0} + f_{IF}\check{t}_{r,S}^k + \phi_{r,NCO}^k(\check{t}_{r,S}^k) - \phi_0^k)}_{\text{receiver and satellite bias}} + \lambda N_r^k + \varepsilon_r^k\end{aligned} \tag{2.25}$$

The model shows that in the IF case the biases introduced depend either on the receiver or on the satellite and also on both together. If we can't compensate at least the biases depending on the satellite and the receiver, it won't be possible to resolve the carrier phase ambiguity as integer, without an additional correction of those biases. That will be another requirement for our receiver later. That's why we come back to the aspect mentioned on page 11 that the selection of the NCO initialization phase $\phi^k_{r,NCO}(\check{t}^{k_r,S})$ is crucial for integer ambiguity resolution. To solve this problem, it is suggested to initialize the NCO phase with a global phase accumulator to make the bias only receiver dependent.

$$\phi^k_{r,NCO}(\check{t}^k_{r,S}) := -\left(f_{IF}\check{t}^k_{r,S} + \phi_{r,GLOBAL}(\check{t}_{r,0})\right) \tag{2.26}$$

That obtains an observation equation with biases only depending either on the receiver or on the satellite.That could be easily removed by differencing like shown in subsection 2.3. There is another possibility to directly drop the receiver dependent biases. You can compensate the phase of the global phase accumulator $\phi_{r,GLOBAL}(\check{t}_{r,0})$ with the zero phase of the mixer $\phi_{r,MIX0}$ in a way that they cancel out in the observation equation:

$$\begin{aligned}\lambda\tilde{\phi}^k_r(\check{t}_{r,RX}) =& r^k_r(\check{t}^k_{r,RX}) + c(\delta\tau_r - \delta\tau^k) - I^k_r + T^k_r \\ &+ \underbrace{\lambda\left(\phi_{r,MIX0} - \phi_{r,GLOBAL}(\check{t}_{r,0}) - \phi^k_0\right)}_{\text{receiver and satellite bias}} + \lambda N^k_r + \varepsilon^k_r\end{aligned} \tag{2.27}$$

2.3 Difference GNSS Models

This thesis deals with relative positioning aspects and for this case single and double differences are very interesting. On the one hand they remove common mode errors and on the other hand we will see that with some receiver requirements they make it possible to resolve the integer ambiguity without accounting for additional biases dependent of the receiver and the satellite, but caused only by the receiver design. For this section we assume the following observation equations. In relation to the standard observation equation (2.4) and (2.5) mentioned at the beginning of this chapter they contain terms for receiver dependent b_r, satellite dependent b^k and receiver and satellite dependent b_r^k biases. With that we can show in which cases they drop out.

$$\rho_r^k = r_r^k(\check{t}_{r,RX}^k) + c(\delta\tau_r - \delta\tau^k) + I_r^k + T_r^k + b^k + b_r + b_r^k + \eta_r^k \tag{2.28}$$

$$\lambda\phi_r^k = r_r^k(\check{t}_{r,RX}^k) + c(\delta\tau_r - \delta\tau^k) - I_r^k + T_r^k + \beta^k + \beta_r + \beta_r^k + \lambda N_r^k + \varepsilon_r^k \tag{2.29}$$

2.3.1 Single Difference

We define the single difference as the difference between the measurement of the signal from the same satellite k taken from two different receivers $r = \{1, 2\}$ at the same instant of time. With the single difference operator $\Delta()_{12}^k = ()_1^k - ()_2^k$ we can see:

$$\Delta\rho_{12}^k = \Delta r_{12}^k + c\Delta\tau_{12} + \Delta I_{12}^k + \Delta T_{12}^k + \Delta b_{12} + \Delta b_{12}^k + \Delta\eta_{12}^k \tag{2.30}$$

$$\Delta\phi_{12}^k = \Delta r_{12}^k + c\Delta\tau_{12} - \Delta I_{12}^k + \Delta T_{12}^k + \Delta\beta_{12} + \Delta\beta_{12}^k + \lambda\Delta N_{12}^k + \Delta\epsilon_{12}^k \tag{2.31}$$

The single difference removes the satellite clock error $\delta\tau^k$ and the satellite biases b^k common to the measurements of both receivers. In the special case of a short baseline one can assume that the satellite unit vectors for satellite k and receiver $r = \{1, 2\}$ are the same $\vec{e}^k = \vec{e}_1^k(\check{t}_{1,RX}^k) \approx \vec{e}_2^k(\check{t}_{2,RX}^k)$. Note that this assumption also requires small receiver differential clock offsets, because otherwise the satellite movement during that time period causes the estimated satellite positions to differ from each other and makes the assumption invalid.

3rd Requirement: The receiver differential time error $\Delta\tau_{12} = \tau_1 - \tau_2$ has to be sufficiently small, so that the movement of the satellite during that interval could be neglected and the following assumption could be used $\vec{e}^k = \vec{e}_1^k(\check{t}_{1,RX}^k) \approx \vec{e}_2^k(\check{t}_{2,RX}^k)$.

With this assumption we can formulate

$$\Delta r_{12}^k = (\vec{e}^k)^T(\vec{x}_1 - \vec{x}_2) = (\vec{e}^k)^T\vec{\xi}$$

with explicitly dropping the time relationship, due to the assumption.

2.3.2 Double Difference

We define the double difference as the difference between the single difference for satellite k with that of satellite l at the same instant of time. We get the following equations with the double difference operator defined as $\Delta\nabla()_{12}^{kl} = \Delta()_{12}^k - \Delta()_{12}^l = ()_1^k - ()_2^k - ()_1^l + ()_2^l$:

$$\Delta\nabla\rho_{12}^{kl} = \Delta\nabla r_{12}^{kl} + \Delta\nabla I_{12}^{kl} + \Delta\nabla T_{12}^{kl} + \Delta\nabla b_{12}^{kl} + \Delta\nabla\eta_{12}^{kl} \tag{2.32}$$

$$\Delta\nabla\phi_{12}^{kl} = \Delta\nabla r_{12}^{kl} - \Delta\nabla I_{12}^{kl} + \Delta\nabla T_{12}^{kl} + \Delta\nabla\beta_{12}^{kl} + \lambda\Delta\nabla N_{12}^{kl} + \Delta\nabla\epsilon_{12}^k \tag{2.33}$$

The double difference removes the receiver clock difference error $\Delta\delta\tau_{12}$ and the receiver differential bias Δb_r common to the single difference of both satellites. In the special case of a short baseline one can assume that the differential ionospheric $\Delta\nabla I_{12}^{kl}$ and tropospheric $\Delta\nabla T_{12}^{kl}$ delays can be neglected. Further one can assume as done before that the satellite unit vectors for satellite k and receiver $r = \{1, 2\}$ are the same. That means $\vec{e}^{\,k} = \vec{e}_1^{\,k}(\check{t}_{1,RX}^{k}) \approx \vec{e}_2^{\,k}(\check{t}_{2,RX}^{k})$ and the same is true for satellite l. Again remember please, that the receiver time difference has to be the same.

$$\begin{aligned}
\triangle r_{12}^{k} &= (\vec{e}^{\,k})^T(\vec{x}_1 - \vec{x}_2) = (\vec{e}^{\,k})^T\vec{\xi} \\
\triangle r_{12}^{l} &= (\vec{e}^{\,l})^T(\vec{x}_1 - \vec{x}_2) = (\vec{e}^{\,l})^T\vec{\xi} \\
\Delta\nabla r_{12}^{kl} &= (\vec{e}^{\,k})^T\vec{\xi} - (\vec{e}^{\,l})^T\vec{\xi} = (\vec{e}^{\,k} - \vec{e}^{\,l})^T\vec{\xi}
\end{aligned}$$

For this case the equations (2.32) and (2.33) can be simplified to the following equations:

$$\Delta\nabla\rho_{12}^{kl} = (\vec{e}^{\,k} - \vec{e}^{\,l})^T\vec{\xi} + \Delta\nabla b_{12}^{kl} + \Delta\nabla\eta_{12}^{kl} \tag{2.34}$$

$$\Delta\nabla\phi_{12}^{kl} = (\vec{e}^{\,k} - \vec{e}^{\,l})^T\vec{\xi} + \Delta\nabla\beta_{12}^{kl} + \lambda\Delta\nabla N_{12}^{kl} + \Delta\nabla\epsilon_{12}^{k} \tag{2.35}$$

That equation makes it possible to formulate our last receiver requirement.

4th Requirement: The receiver generated signal should not contain biases depending on the satellite and the receiver for which at least the double difference could be neglected. Otherwise the integer ambiguity could be resolved as integer only by additional corrections of remaining biases. Therefore the receiver design should not introduce such biases in the measurement.

2.4 Summary: Receiver Requirements for Double Difference Integer Ambiguity Resolution

Now we summarize our receiver requirements. Please note, that they could also be found in the literature e.g. in [12].

1st Requirement: The receiver detects and corrects phase jumps of $\delta\phi = \pm 0.5$ cycles due to the modulated navigation message.

2nd Requirement: The PLL of the receiver should integrate the NCO phase $\phi_{r,NCO}^{k}(\check{t}_{r,RX}^{k})$ and store the number of full cycles of its generated reference signal defined as the integer component of the NCO phase, noted as $L_r^k(\check{t}_{r,RX}^{k})$.

3rd Requirement: The receiver differential time error $\Delta\tau_{12} = \tau_1 - \tau_2$ has to be sufficiently small, so that the movement of the satellite during that interval could be neglected and the following assumption could be used $\vec{e}^{\,k} = \vec{e}_1^{\,k}(\check{t}_{1,RX}^{k}) \approx \vec{e}_2^{\,k}(\check{t}_{2,RX}^{k})$.

4th Requirement: The receiver generated signal should not contain biases depending on the satellite and the receiver for which at least the double difference could be neglected. Otherwise the integer ambiguity could be resolved as integer only by additional corrections of remaining biases.

2.5 General linear(ized) GNSS Model formulation

Despite the fact that we derive the following notation only from double difference measurements it should be clear that every linearized GNSS problem can be formulated in matrix vector notation of the following type[8].

$$\boldsymbol{\Psi} = \mathbf{H}\boldsymbol{\xi} + \mathbf{A}\boldsymbol{N} + \boldsymbol{\eta} \tag{2.36}$$

With $\boldsymbol{\Psi}$ as the vector containing all observations, the vector $\boldsymbol{\xi}$ contains the unknown real valued parameters, in our case that will only be the three components of the baseline vector $\Delta\vec{\boldsymbol{x}}_{12}$. The unknown integer valued parameters are contained in $\boldsymbol{N}$. The vector $\boldsymbol{\eta}$ describes the measurement noise and all unmodeled errors. The two design matrices describe the known relationship between either $\boldsymbol{\xi}$ or $\boldsymbol{N}$ and $\boldsymbol{\Psi}$. The matrix $\mathbf{H}$ is called the geometry matrix because it contains the satellite receiver line-of-sight unit vectors.

If we want to describe the baseline $\Delta\vec{\boldsymbol{x}}_{12}$ instead of Cartesian coordinates in spherical coordinates of the local East-North-Up Coordinate Frame (ENU) coordinate system with ν_1, ν_2 and l, we have to add the following nonlinear transformation to our model:

$$\Delta\vec{\boldsymbol{x}}_{12} = \boldsymbol{r}(\nu_1, \nu_2)l = \begin{bmatrix} \cos(\nu_1)\sin(\nu_2) \\ \cos(\nu_1)\sin(\nu_2) \\ \sin(\nu_1) \end{bmatrix} l \tag{2.37}$$

We have K available satellites indexed with $k \in \{1, ..., K\}$ and we choose the m-th satellite as our reference satellite to form all double differences in relation to this satellite.

2.5.1 Single Epoch Model with only Carrier phase Measurement

$$\underbrace{\begin{bmatrix} \lambda\Delta\nabla\phi_{12}^{1m} \\ \vdots \\ \lambda\Delta\nabla\phi_{12}^{(m-1)m} \\ \lambda\Delta\nabla\phi_{12}^{(m+1)m} \\ \vdots \\ \lambda\Delta\nabla\phi_{12}^{Km} \end{bmatrix}}_{\boldsymbol{\Psi}} = \underbrace{\begin{bmatrix} (\vec{\boldsymbol{e}}^{1m})^T \\ \vdots \\ (\vec{\boldsymbol{e}}^{(m-1)m})^T \\ (\vec{\boldsymbol{e}}^{(m+1)m})^T \\ \vdots \\ (\vec{\boldsymbol{e}}^{Km})^T \end{bmatrix}}_{\boldsymbol{H}} \underbrace{\Delta\vec{\boldsymbol{x}}_{12}}_{\boldsymbol{\xi}} + \underbrace{\begin{bmatrix} \lambda & & & & \\ & \ddots & & & \\ & & \ddots & & \\ & & & \ddots & \\ & & & & \lambda \end{bmatrix}}_{\boldsymbol{A}} \underbrace{\begin{bmatrix} \Delta\nabla N_{12}^{1m} \\ \vdots \\ \Delta\nabla N_{12}^{(m-1)m} \\ \Delta\nabla N_{12}^{(m+1)m} \\ \vdots \\ \Delta\nabla N_{12}^{Km} \end{bmatrix}}_{\boldsymbol{N}} + \underbrace{\begin{bmatrix} \Delta\nabla\varepsilon_{12}^{1m} \\ \vdots \\ \Delta\nabla\varepsilon_{12}^{(m-1)m} \\ \Delta\nabla\varepsilon_{12}^{(m+1)m} \\ \vdots \\ \Delta\nabla\varepsilon_{12}^{Km} \end{bmatrix}}_{\boldsymbol{\eta}} \tag{2.38}$$

The dimensions are:

$$\begin{aligned} \dim(\boldsymbol{\Psi}) &= (K-1)\times 1 & \dim(\boldsymbol{H}) &= (K-1)\times 3 \\ \dim(\boldsymbol{\xi}) &= 3\times 1 & \dim(\boldsymbol{A}) &= (K-1)\times(K-1) \\ \dim(\boldsymbol{N}) &= (K-1)\times 1 & \dim(\boldsymbol{\eta}) &= (K-1)\times 1 \end{aligned} \tag{2.39}$$

2.5.2 Single Epoch Model with Code and Carrier-Phase Measurement

$$\underbrace{\begin{bmatrix} \lambda\Delta\nabla\phi_{12}^{1m} \\ \vdots \\ \lambda\Delta\nabla\phi_{12}^{(m-1)m} \\ \lambda\Delta\nabla\phi_{12}^{(m+1)m} \\ \vdots \\ \lambda\Delta\nabla\phi_{12}^{Km} \\ \hline \Delta\nabla\rho_{12}^{1m} \\ \vdots \\ \Delta\nabla\rho_{12}^{(m-1)m} \\ \Delta\nabla\rho_{12}^{(m+1)m} \\ \vdots \\ \Delta\nabla\rho_{12}^{Km} \end{bmatrix}}_{\boldsymbol{\Psi}} = \underbrace{\begin{bmatrix} (\vec{\boldsymbol{e}}^{1m})^T \\ \vdots \\ (\vec{\boldsymbol{e}}^{(m-1)m})^T \\ (\vec{\boldsymbol{e}}^{(m+1)m})^T \\ \vdots \\ (\vec{\boldsymbol{e}}^{Km})^T \\ \hline (\vec{\boldsymbol{e}}^{1m})^T \\ \vdots \\ (\vec{\boldsymbol{e}}^{(m-1)m})^T \\ (\vec{\boldsymbol{e}}^{(m+1)m})^T \\ \vdots \\ (\vec{\boldsymbol{e}}^{Km})^T \end{bmatrix}}_{\boldsymbol{H}} \underbrace{\Delta\vec{\boldsymbol{x}}_{12}}_{\boldsymbol{\xi}} + \underbrace{\begin{bmatrix} \lambda & & \\ & \ddots & \\ & & \lambda \\ \hline & & \\ & 0 & \\ & & \end{bmatrix}}_{\boldsymbol{A}} \underbrace{\begin{bmatrix} \Delta\nabla N_{12}^{1m} \\ \vdots \\ \Delta\nabla N_{12}^{(m-1)m} \\ \Delta\nabla N_{12}^{(m+1)m} \\ \vdots \\ \Delta\nabla N_{12}^{Km} \end{bmatrix}}_{\boldsymbol{N}} + \underbrace{\begin{bmatrix} \Delta\nabla\varepsilon_{12}^{1m} \\ \vdots \\ \Delta\nabla\varepsilon_{12}^{(m-1)m} \\ \Delta\nabla\varepsilon_{12}^{(m+1)m} \\ \vdots \\ \Delta\nabla\varepsilon_{12}^{Km} \\ \hline \Delta\nabla\eta_{12}^{1m} \\ \vdots \\ \Delta\nabla\eta_{12}^{(m-1)m} \\ \Delta\nabla\eta_{12}^{(m+1)m} \\ \vdots \\ \Delta\nabla\eta_{12}^{Km} \end{bmatrix}}_{\boldsymbol{\eta}} \tag{2.40}$$

The dimensions are:

$$\begin{aligned} &\dim(\boldsymbol{\Psi}) = (2\cdot(K-1))\times 1 && \dim(\boldsymbol{H}) = (2\cdot(K-1))\times 3 \\ &\dim(\boldsymbol{\xi}) = 3\times 1 && \dim(\boldsymbol{A}) = (2\cdot(K-1))\times(K-1) \\ &\dim(\boldsymbol{N}) = (K-1)\times 1 && \dim(\boldsymbol{\eta}) = (2\cdot(K-1))\times 1 \end{aligned} \tag{2.41}$$

2.5.3 Multi Epoch Model with Code and/or Carrier-Phase Measurement

With $\tilde{\Psi}$ $\tilde{H}$ $\tilde{A}$ $\tilde{\eta}$ defined according any single epoch model the multi-epoch model is defined as follows. Please note that the reference satellite m has to be the same in all epochs. And the carrier phase is traced without cycle slip during the period t_1 to t_E with E the number of epochs contained in this model.

$$\underbrace{\begin{bmatrix} \tilde{\boldsymbol{\Psi}}(t_1) \\ \vdots \\ \tilde{\boldsymbol{\Psi}}(t_E) \end{bmatrix}}_{\boldsymbol{\Psi}} = \underbrace{\begin{bmatrix} \tilde{\boldsymbol{H}}(t_1) & & \\ & \ddots & \\ & & \tilde{\boldsymbol{H}}(t_E) \end{bmatrix}}_{\boldsymbol{H}} \underbrace{\begin{bmatrix} \tilde{\boldsymbol{\xi}}(t_1) \\ \vdots \\ \tilde{\boldsymbol{\xi}}(t_E) \end{bmatrix}}_{\boldsymbol{\xi}} + \underbrace{\begin{bmatrix} \tilde{\boldsymbol{A}}(t_1) \\ \vdots \\ \tilde{\boldsymbol{A}}(t_E) \end{bmatrix}}_{\boldsymbol{A}} \underbrace{\begin{bmatrix} \Delta\nabla N_{12}^{1m} \\ \vdots \\ \Delta\nabla N_{12}^{(m-1)m} \\ \Delta\nabla N_{12}^{(m+1)m} \\ \vdots \\ \Delta\nabla N_{12}^{Km} \end{bmatrix}}_{\boldsymbol{N}} + \underbrace{\begin{bmatrix} \tilde{\boldsymbol{\eta}}(t_1) \\ \vdots \\ \tilde{\boldsymbol{\eta}}(t_E) \end{bmatrix}}_{\boldsymbol{\eta}} \tag{2.42}$$

With K the number of satellites E the number of epochs and the definition of

$$p := \begin{cases} 2E(K-1), & \text{for code and phase measurements} \\ E(K-1), & \text{for phase only measurements} \end{cases} \tag{2.43}$$

the dimensions are:

$$\begin{aligned} &\dim(\boldsymbol{\Psi}) = p\times 1 && \dim(\boldsymbol{H}) = p\times(3\cdot E) \\ &\dim(\boldsymbol{\xi}) = (3\cdot E)\times 1 && \dim(\boldsymbol{A}) = p\times(K-1) \\ &\dim(\boldsymbol{N}) = (K-1)\times 1 && \dim(\boldsymbol{\eta}) = p\times 1 \end{aligned} \tag{2.44}$$

3. Ambiguity Resolution Algorithms

In the previous chapter we defined our model and got to a general matrix notation in (2.36) which is shown here again.

$$\boldsymbol{\Psi} = \mathbf{H}\boldsymbol{\xi} + \mathbf{A}\boldsymbol{N} + \boldsymbol{\eta}$$

That will be the starting point for this chapter. The first section describes the origin of the standard integer least squares problem, as a derivation of an Maximum Likelihood (ML) estimator. Further the first section mentions the orthogonal decomposition of this problem. The second section introduces a method which uses soft constrains as additional a priori knowledge. The derivation from an Maximum A Posteriori Probability (MAP) estimator is shown as well as the current soft constrained integer search is explained. This is the method introduced by Henkel and Jurkowski in [6][7]. As a further development of the current soft constrained integer ambiguity resolution algorithm the third section introduces an improvement of this method. The a priori knowledge for the improved MAP estimator is based on the assumption of the a priori knowledge formulated in the position domain instead of in the spherical domain. Also the soft constrained tree search is improved.

3.1 Standard Integer Least Squares Problem

In the case of no statistical knowledge about the unknown parameters $\boldsymbol{\xi}$ and $\boldsymbol{N}$, the estimation problem could be formulated as an ML estimator which tries to find the baseline parameter $\boldsymbol{\xi}$ and ambiguities $\boldsymbol{N}$, which had generated the measurements with the highest probability[13]. Further to simplify the notation we drop the dimensions on the right hand side. Only in cases where this isn't true we write the long version.

$$\max_{\boldsymbol{\xi}\in\mathbb{R}^3,\boldsymbol{N}\in\mathbb{Z}^p} p(\boldsymbol{\Psi}|\boldsymbol{\xi},\boldsymbol{N}) = \max_{\boldsymbol{\xi},\boldsymbol{N}} p(\boldsymbol{\Psi}|\boldsymbol{\xi},\boldsymbol{N}) \tag{3.1}$$

This term $p(\boldsymbol{\Psi}|\boldsymbol{\xi},\boldsymbol{N})$ like mentioned above is the conditional probability for $\boldsymbol{\Psi}$ under side conditions that the baseline parameters $\boldsymbol{\xi}$ and the ambiguities are known. That describes the measurement noise, which is assumed to be Gaussian. With the next few steps one can derive the so-called integer least squares criteria[8]. Please note, that the dimension p is defind in the previous chapter in equation (2.43).

$$\max_{\boldsymbol{\xi},\boldsymbol{N}} p(\boldsymbol{\Psi}|\boldsymbol{\xi},\boldsymbol{N}) = \max_{\boldsymbol{\xi},N} \frac{1}{\sqrt{(2\pi)^p|\boldsymbol{\Sigma}|}} \exp\Big(-\frac{1}{2}\|\boldsymbol{\Psi}-\boldsymbol{H}\boldsymbol{\xi}-\boldsymbol{A}\boldsymbol{N}\|^2_{\boldsymbol{\Sigma}^{-1}}\Big) \tag{3.2}$$

$$= \min_{\boldsymbol{\xi},N} \|\boldsymbol{\Psi}-\boldsymbol{H}\boldsymbol{\xi}-\boldsymbol{A}\boldsymbol{N}\|^2_{\boldsymbol{\Sigma}^{-1}} \tag{3.3}$$

In the text book [8] the authors introduced an orthogonal decomposition of this problem. You can find an explicit derivation of this decomposition using the same notation as in this thesis in [6]. For that reason it is not derived in this thesis again but the results are mentioned in the following part. In the first step the solution is define which assumes all unknowns as real valued that means $\boldsymbol{\xi} \in \mathbb{R}^3$

and $\boldsymbol{N} \in \mathbb{R}^p$ as the float least-squares solution.

$$\begin{bmatrix} \hat{\boldsymbol{\xi}} \\ \hat{\boldsymbol{N}} \end{bmatrix} = \arg \min_{\boldsymbol{\xi} \in \mathbb{R}^3, \boldsymbol{N} \in \mathbb{R}^p} \|\boldsymbol{\Psi} - \boldsymbol{H}\boldsymbol{\xi} - \boldsymbol{A}\boldsymbol{N}\|^2_{\boldsymbol{\Sigma}^{-1}} \tag{3.4}$$

In a second step the following definitions for an orthogonal projection are applied:

$$\begin{aligned} \boldsymbol{P}_H &:= \boldsymbol{H}(\boldsymbol{H}^T\boldsymbol{\Sigma}^{-1}\boldsymbol{H})^{-1}\boldsymbol{H}^T\boldsymbol{\Sigma}^{-1} \\ \boldsymbol{P}_H^{\perp} &:= \mathbf{1} - \boldsymbol{P}_H \\ \bar{\boldsymbol{A}} &:= \boldsymbol{P}_H^{\perp} \cdot \boldsymbol{A} \\ \boldsymbol{P}_{\bar{\boldsymbol{A}}} &:= \bar{\boldsymbol{A}}(\bar{\boldsymbol{A}}^T\boldsymbol{\Sigma}^{-1}\bar{\boldsymbol{A}})^{-1}\bar{\boldsymbol{A}}^T\boldsymbol{\Sigma}^{-1} \\ \boldsymbol{P}_{\bar{\boldsymbol{A}}}^{\perp} &:= \mathbf{1} - \boldsymbol{P}_{\bar{\boldsymbol{A}}} \end{aligned}$$

In accordance with [6], the solution of $\boldsymbol{\xi}$ obtained with one known vector $\boldsymbol{N}$ is interpreted as follows:

$$\check{\boldsymbol{\xi}}(\boldsymbol{N}) = \arg\min_{\boldsymbol{\xi}} \|\boldsymbol{\Psi} - \boldsymbol{A}\boldsymbol{N} - \boldsymbol{H}\boldsymbol{\xi}\|^2_{\boldsymbol{\Sigma}^{-1}} = (\boldsymbol{H}^T\boldsymbol{\Sigma}^{-1}\boldsymbol{H})^{-1}\boldsymbol{H}^T\boldsymbol{\Sigma}^{-1}(\boldsymbol{\Psi} - \boldsymbol{A}\boldsymbol{N}) \tag{3.5}$$

The definition of the variance-/covariance matrices are transformed in the following way:

$$\boldsymbol{\Sigma}_{\hat{\boldsymbol{N}}}{}^{-1} := (\bar{\boldsymbol{A}}^T\boldsymbol{\Sigma}^{-1}\bar{\boldsymbol{A}})^{-1} \tag{3.6}$$

$$\boldsymbol{\Sigma}^{-1}_{\check{\boldsymbol{\xi}}(\boldsymbol{N})} := (\boldsymbol{H}^T\boldsymbol{\Sigma}^{-1}\boldsymbol{H})^{-1} \tag{3.7}$$

With this projection one could show that the minimization problem in (3.3) could be formulated in dependence of the float solution mentioned in equation (3.4) and $\hat{\boldsymbol{\xi}}(\boldsymbol{N})$ defined in (3.5). That is the so-called fixed solution where there are $\check{\boldsymbol{\xi}} \in \mathbb{R}^3$ and $\check{\boldsymbol{N}} \in \mathbb{Z}^p$.

$$\begin{bmatrix} \check{\boldsymbol{\xi}} \\ \check{\boldsymbol{N}} \end{bmatrix} = \arg\min_{\boldsymbol{N}}\Big(\|\boldsymbol{\Psi} - \boldsymbol{H}\hat{\boldsymbol{\xi}} - \boldsymbol{A}\hat{\boldsymbol{N}}\|^2_{\boldsymbol{\Sigma}^{-1}} + \|\hat{\boldsymbol{N}} - \boldsymbol{N}\|^2_{\boldsymbol{\Sigma}^{-1}_{\hat{\boldsymbol{N}}}} + \min_{\boldsymbol{\xi}} \|\check{\boldsymbol{\xi}}(\boldsymbol{N}) - \boldsymbol{\xi}\|^2_{\boldsymbol{\Sigma}^{-1}_{\check{\boldsymbol{\xi}}(\boldsymbol{N})}}\Big) \tag{3.8}$$

The first term is the residual error vector of the float solution which is independent of $\check{\boldsymbol{\xi}}$ and $\check{\boldsymbol{N}}$ and thus it is not reducible. One could drop this term for the further minimization. We now have instead of one minimization problem over two variables two cascaded minimizations each over one variable:

$$\begin{bmatrix} \check{\boldsymbol{\xi}} \\ \check{\boldsymbol{N}} \end{bmatrix} = \arg\min_{\boldsymbol{N}}\Big(\|\hat{\boldsymbol{N}} - \boldsymbol{N}\|^2_{\boldsymbol{\Sigma}^{-1}_{\hat{\boldsymbol{N}}}} + \min_{\boldsymbol{\xi}} \|\check{\boldsymbol{\xi}}(\boldsymbol{N}) - \boldsymbol{\xi}\|^2_{\boldsymbol{\Sigma}^{-1}_{\check{\boldsymbol{\xi}}(\boldsymbol{N})}}\Big) \tag{3.9}$$

For this case the minimization could be separated and therefore performed in the following two steps sequentially. That is possible because for every $\boldsymbol{N}$ a $\boldsymbol{\xi}$ could be found which makes the inner minimization to zero. That is the case, if $\boldsymbol{\xi} = \check{\boldsymbol{\xi}}(\boldsymbol{N})$ is chosen as minimizer.

$$\check{\boldsymbol{N}} = \arg\min_{\boldsymbol{N}}\Big(\|\hat{\boldsymbol{N}} - \boldsymbol{N}\|^2_{\boldsymbol{\Sigma}^{-1}_{\hat{\boldsymbol{N}}}}\Big) \tag{3.10}$$

$$\check{\boldsymbol{\xi}} = \check{\boldsymbol{\xi}}(\check{\boldsymbol{N}}) = \arg\min_{\boldsymbol{\xi}}\Big(\|\check{\boldsymbol{\xi}}(\check{\boldsymbol{N}}) - \boldsymbol{\xi}\|^2_{\boldsymbol{\Sigma}^{-1}_{\check{\boldsymbol{\xi}}(\check{\boldsymbol{N}})}}\Big) = (\boldsymbol{H}^T\boldsymbol{\Sigma}^{-1}\boldsymbol{H})^{-1}\boldsymbol{H}^T\boldsymbol{\Sigma}^{-1}(\boldsymbol{\Psi} - \boldsymbol{A}\check{\boldsymbol{N}}) \tag{3.11}$$

3.2 Soft Constrained Ambiguity Resolution - Spherical A Priori Knowledge

3.2.1 Maximum A Posteriori Probability Estimator

Like mentioned in the introduction Henkel and Jurkowski developed in [6][7] an MAP estimator which uses statistical a priori knowledge of the baseline length as well as the pitch and heading angels. In the following section the method is derived in a similar way like Henkel and Jurkowski do it in [7] but with some changes due to accord with the rest of the thesis. Remember that the baseline could be described with the transformation from (2.37) in spherical coordinates. This description is used in the following derivation.

Despite the ML estimator shown under section 3.1, the MAP estimator maximizes the probability of ν_1 ν_2,l and $\boldsymbol{N}$ if a measurement $\boldsymbol{\Psi}$ is given. The MAP estimator is defined as follows and reformulated with the rule of Bayes and the assumption of statistical independent a priori knowledge of the baseline parameters.

$$\max_{\nu_1,\nu_2,l,N} p(\nu_1,\nu_2,l,\boldsymbol{N}|\boldsymbol{\Psi}) = \max_{\nu_1,\nu_2,l,\boldsymbol{N}} p(\boldsymbol{\Psi}|\nu_1,\nu_2,l,\boldsymbol{N}) \cdot \frac{p(\nu_1,\nu_2,l,\boldsymbol{N})}{p(\boldsymbol{\Psi})} \tag{3.12}$$

$$= \max_{\nu_1,\nu_2,l,\boldsymbol{N}} p(\boldsymbol{\Psi}|\nu_1,\nu_2,l,\boldsymbol{N}) \cdot \frac{p(\nu_1)p(\nu_2)p(l)p(\boldsymbol{N})}{p(\boldsymbol{\Psi})} \tag{3.13}$$

First it should be clarified what the different terms on the right hand side in (3.13) mean. The first term $p(\boldsymbol{\Psi}|\nu_1,\nu_2,l,\boldsymbol{N})$ is the conditional probability for the measurement $\boldsymbol{Psi}$ under the side condition that the baseline parameters ν_1,ν_2 and l as well as the integer ambiguity vector $\boldsymbol{N}$ is known. That describes the measurement noise, which is assumed to be Gaussian:

$$p(\boldsymbol{\Psi}|\nu_1,\nu_2,l,\boldsymbol{N}) = \frac{1}{\sqrt{(2\pi)^p|\boldsymbol{\Sigma}|}} \exp\Big(-\frac{1}{2}\|\boldsymbol{\Psi} - \boldsymbol{Hr}(\nu_1,\nu_2)l - \boldsymbol{AN}\|^2_{\boldsymbol{\Sigma}^{-1}}\Big) \tag{3.14}$$

The matrix $\boldsymbol{\Sigma}$ is the variance/-covariance matrix of the measurement and p is the dimension of the distribution and in our case defined in equation (2.43). The first term only would lead to the prior described ML estimator. The additional second term on the right hand side has in its nominator the joint probability distribution for the statistical independent a piori knowledge of the baseline $p(\nu_1,\nu_2,l,N) = p(\nu_1)p(\nu_2)p(l)p(\boldsymbol{N})$, where the individual terms are assumed to be Gaussian distributed, except for $p(\boldsymbol{N})$. The notations $\bar{\nu}_x$ for $x \in \{1,2\}$ and $\bar{l}$ in the equations (3.15) and (3.16) stand for the true baseline parameters.

$$p(\nu_x) = \frac{1}{\sqrt{2\pi\sigma^2_{\bar{\nu}_x}}} \exp\Big(-\frac{(\nu_x - \bar{\nu}_x)^2}{2\sigma^2_{\bar{\nu}_x}}\Big) \tag{3.15}$$

$$p(l) = \frac{1}{\sqrt{2\pi\sigma^2_{\bar{l}}}} \exp\Big(-\frac{(l - \bar{l})^2}{2\sigma^2_{\bar{l}}}\Big) \tag{3.16}$$

The only exception is the probability $p(\boldsymbol{N})$. Due to the fact that we don't have any a priori knowledge, every $\boldsymbol{N}$ contained in $\Omega \subseteq \mathbb{Z}^p$ has the same probability. With Ω the set of all integer vectors of dimension p and $|\Omega|$ as the cardinal number, one could formulate the discrete distribution of $p(\boldsymbol{N})$ as:

$$p(\boldsymbol{N}) = \begin{cases} \frac{1}{|\Omega|} =: n, & \boldsymbol{N} \in \Omega \\ 0, & \boldsymbol{N} \notin \Omega \end{cases} \tag{3.17}$$

The denominator of the second term in (3.13) can be calculated as the marginal probability. It can be shown that this integration and sum leads to a constant c:

$$p(\boldsymbol{\Psi}) = \sum_{\boldsymbol{N}\in\Omega} \int_{-\infty}^{\infty} \int_{-\infty}^{\infty} \int_{-\infty}^{\infty} p(\boldsymbol{\Psi}|\nu_1,\nu_2,l,\boldsymbol{N}) p(\nu_1)p(\nu_2)p(l)p(\boldsymbol{N})\; d\nu_1 d\nu_2 dl = c = \text{const.} \tag{3.18}$$

Because $p(\boldsymbol{\Psi})$ is independent of our parameters we can neglect it for the maximization. With this information Henkel and Jurkowski derived the cost function $J(\nu_1,\nu_2,l,\boldsymbol{N})$ with the following steps.

$$\begin{aligned}
&\max_{\nu_1,\nu_2,l,\boldsymbol{N}} p(\nu_1,\nu_2,l,N|\boldsymbol{\Psi}) \\
&= \max_{\nu_1,\nu_2,l,\boldsymbol{N}} p(\boldsymbol{\Psi}|\nu_1,\nu_2,l,N)p(\nu_1)p(\nu_2)p(l) \\
&= \max_{\nu_1,\nu_2,l,\boldsymbol{N}} \exp\Big(-\frac{1}{2}\|\boldsymbol{\Psi}-\boldsymbol{H}\boldsymbol{r}(\nu_1,\nu_2)l-\boldsymbol{A}\boldsymbol{N}\|^2_{\boldsymbol{\Sigma}^{-1}}\Big)\exp\Big(-\frac{(\nu_1-\bar{\nu}_1)^2}{2\sigma^2_{\bar{\nu}_1}}\Big)\exp\Big(-\frac{(\nu_2-\bar{\nu}_2)^2}{2\sigma^2_{\bar{\nu}_2}}\Big)\exp\Big(-\frac{(l-\bar{l})^2}{2\sigma^2_{\bar{l}}}\Big) \\
&= \min_{\nu_1,\nu_2,l,\boldsymbol{N}} \Big(\|\boldsymbol{\Psi}-\boldsymbol{H}\boldsymbol{r}(\nu_1,\nu_2)l-\boldsymbol{A}\boldsymbol{N}\|^2_{\boldsymbol{\Sigma}^{-1}} + \frac{(\nu_1-\bar{\nu}_1)^2}{\sigma^2_{\bar{\nu}_1}} + \frac{(\nu_2-\bar{\nu}_2)^2}{\sigma^2_{\bar{\nu}_2}} + \frac{(l-\bar{l})^2}{\sigma^2_{\bar{l}}}\Big)
\end{aligned} \tag{3.19}$$

With the same orthogonal decomposition as in section 3.1 we obtain:

$$\begin{aligned}
&\max_{\nu_1,\nu_2,l,\boldsymbol{N}} p(\nu_1,\nu_2,l,N|\boldsymbol{\Psi}) \\
&= \min_{\boldsymbol{N}} \Big(\|\hat{\boldsymbol{N}}-\boldsymbol{N}\|^2_{\boldsymbol{\Sigma}^{-1}_{\hat{\boldsymbol{N}}}} + \min_{\nu_1,\nu_2,l} \big(\|\check{\boldsymbol{\xi}}(\boldsymbol{N})-\boldsymbol{\xi}\|^2_{\boldsymbol{\Sigma}^{-1}_{\check{\boldsymbol{\xi}}(\boldsymbol{N})}} + \frac{(\nu_1-\bar{\nu}_1)^2}{\sigma^2_{\bar{\nu}_1}} + \frac{(\nu_2-\bar{\nu}_2)^2}{\sigma^2_{\bar{\nu}_2}} + \frac{(l-\bar{l})^2}{\sigma^2_{\bar{l}}}\big)\Big) \\
&= \max_{\nu_1,\nu_2,l,\boldsymbol{N}} \boldsymbol{J}(\boldsymbol{\Psi},\nu_1,\nu_2,l,\boldsymbol{N})
\end{aligned} \tag{3.20}$$

But in the current case it is not possible to split the minimization in two steps because due to the baseline constraints the minimization over ν_1,ν_2 and l could not be made to zero for any $\boldsymbol{N}$. In consequence the estimation for the spherical baseline parameters and the ambiguity vector has to be performed together starting from equation (3.19). Further it is a non- linear system of equations where we search for the zero of the first derivative. That could be done with the help of e.g. the Gauss-Newton method. The float solution is formulated in the n-th step of the iteration like this [7]:

$$\begin{bmatrix} \hat{\boldsymbol{\nu}}_{\mathbf{1}}{}^{n+1} \\ \hat{\boldsymbol{\nu}}_{\mathbf{1}}{}^{n+1} \\ \hat{\boldsymbol{l}}^{n+1} \\ \hat{\boldsymbol{N}}^{n+1} \end{bmatrix} = \begin{bmatrix} \hat{\boldsymbol{\nu}}_{\mathbf{1}}{}^{n} \\ \hat{\boldsymbol{\nu}}_{\mathbf{1}}{}^{n} \\ \hat{\boldsymbol{l}}^{n} \\ \hat{\boldsymbol{N}}^{n} \end{bmatrix} - \boldsymbol{S}^{-1} \begin{bmatrix} \frac{\partial \boldsymbol{J}}{\partial \nu_1} \\ \frac{\partial \boldsymbol{J}}{\partial \nu_2} \\ \frac{\partial \boldsymbol{J}}{\partial l} \\ \frac{\partial \boldsymbol{J}}{\partial \boldsymbol{N}} \end{bmatrix} \qquad \boldsymbol{S} = \begin{bmatrix} \frac{\partial^2 \boldsymbol{J}}{\partial^2 \nu_1} & \frac{\partial^2 \boldsymbol{J}}{\partial \nu_1 \partial \nu_2} & \frac{\partial^2 \boldsymbol{J}}{\partial \nu_1 \partial l} & \frac{\partial^2 \boldsymbol{J}}{\partial \nu_1 \partial \boldsymbol{N}} \\ \frac{\partial^2 \boldsymbol{J}}{\partial \nu_1 \partial \nu_2} & \frac{\partial^2 \boldsymbol{J}}{\partial^2 \nu_2} & \frac{\partial^2 \boldsymbol{J}}{\partial \nu_2 \partial l} & \frac{\partial^2 \boldsymbol{J}}{\partial \nu_2 \partial \boldsymbol{N}} \\ \frac{\partial^2 \boldsymbol{J}}{\partial \nu_1 \partial l} & \frac{\partial^2 \boldsymbol{J}}{\partial \nu_2 \partial l} & \frac{\partial^2 \boldsymbol{J}}{\partial^2 l} & \frac{\partial^2 \boldsymbol{J}}{\partial l \partial \boldsymbol{N}} \\ \frac{\partial^2 \boldsymbol{J}}{\partial \nu_1 \partial \boldsymbol{N}} & \frac{\partial^2 \boldsymbol{J}}{\partial \nu_2 \partial \boldsymbol{N}} & \frac{\partial^2 \boldsymbol{J}}{\partial l \partial \boldsymbol{N}} & \frac{\partial^2 \boldsymbol{J}}{\partial^2 \boldsymbol{N}} \end{bmatrix} \tag{3.21}$$

3.2.2 Constrained Integer Search

To find a solution for the minimization problem in (3.19) Henkel and Jurkowski developed a soft constrained tree search algorithm which uses the a priori information of the baseline to substantially improve the efficiency [6][7]. We would like to note that the search should be performed on the decorrelated ambiguities like it is introduced with the Least Squares Ambiguity Decorrelation Adjustment (LAMBDA) method to increase the success rate. They introduce the following notation for the tree search. In general, as in the previous sections, K denotes the number of satellites available:

$k \in \{1, ..., K\}$	vertical tree level (number of ambiguities partially fixed)
$c^k \leq K^k$	number of ambiguities at the k-th level
$j_k \in \{1, ..., c^k\}$	indices of all ambiguities at the k-th level
$s^k = \{\check{\boldsymbol{N}}^k_1, ..., \check{\boldsymbol{N}}^k_{c^k}\}$	set of integer candidates at the k-th level

The search aims to find all integer ambiguity vectors which are contained in the initial search ellipsoid[7], defind with:

$$\|\hat{\boldsymbol{N}} - \boldsymbol{N}\|^2_{\boldsymbol{\Sigma}^{-1}_{\hat{\boldsymbol{N}}}} \leq \chi^2 \tag{3.22}$$

With this defined search space the authors derived the following upper and lower bound for the fixing of the ambiguities at the k-th level in the tree search. The conditional ambiguity estimates $\hat{\boldsymbol{N}}^l_{j_l|j_{1,...,l-1}}$ are the result of the bootstrapping solution as well as the standard deviation is determined from the bootstrapping solution, depending on the fixed integers in the branch from the root to the current integer $\hat{\boldsymbol{N}}^l_{j_l}$. The authors further mention that the variances $\sigma^2_{\hat{N}_{l|1,...,l-1}}$ are also known from bootstrapping and as indicated in the index they only depend on the level of the tree. Therefore they are equal for all integer candidates in the set s^k.

$$\|N^k - \hat{N}^k_{j_k|j_{1,...,k-1}}\| \leq \sigma_{\hat{N}_k|j_{1,...,k-1}} \sqrt{\chi^2 - \sum_{l=1}^{k-1} \frac{\left(\hat{N}^l_{j_l} - \hat{N}^l_{j_l|j_{1,...,l-1}}\right)^2}{\sigma^2_{\hat{N}_{l|1,...,l-1}}}} \tag{3.23}$$

The upper and lower bound is derived from this equation:

$$u_{\hat{N}^k_{j_k}} = \hat{N}^k_{j_k|j_{1,...,k-1}} - \sigma_{\hat{N}_k|j_{1,...,k-1}} \sqrt{\chi^2 - \sum_{l=1}^{k-1} \frac{\left(\hat{N}^l_{j_l} - \hat{N}^l_{j_l|j_{1,...,l-1}}\right)^2}{\sigma^2_{\hat{N}_{l|1,...,l-1}}}} \tag{3.24}$$

$$o_{\hat{N}^k_{j_k}} = \hat{N}^k_{j_k|j_{1,...,k-1}} + \sigma_{\hat{N}_k|j_{1,...,k-1}} \sqrt{\chi^2 - \sum_{l=1}^{k-1} \frac{\left(\hat{N}^l_{j_l} - \hat{N}^l_{j_l|j_{1,...,l-1}}\right)^2}{\sigma^2_{\hat{N}_{l|1,...,l-1}}}} \tag{3.25}$$

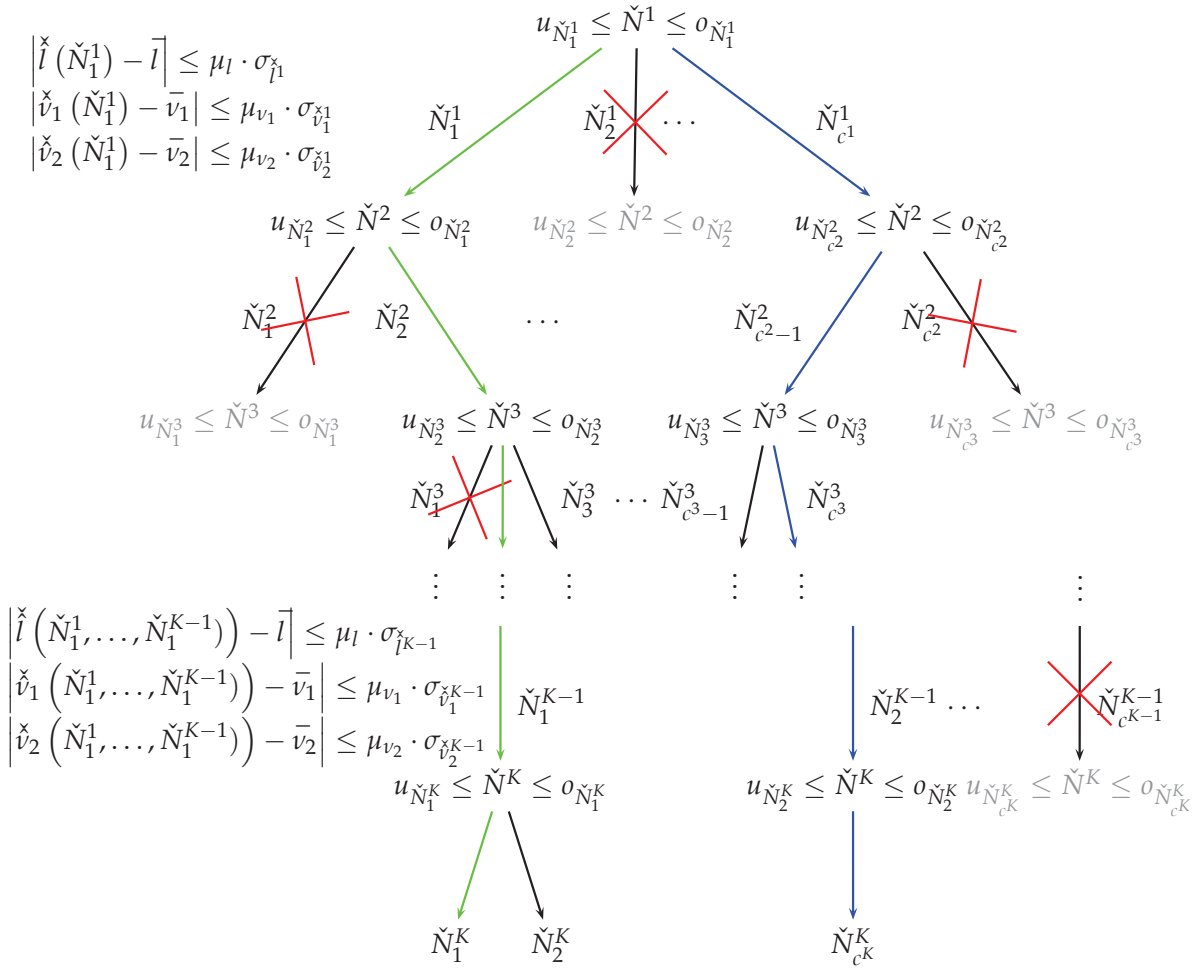

Figure 3.1: Search tree: Constraints on the baseline length and orientation are checked at each path node to reduce the final number of branches. The tightness of the bounds and, thus the efficiency of the search, is determined by the prefactors μ_l,μ_{v_1} and μ_{v_2}[7].(Figure used with permission of Jurkowski P.)

At every node the tree is generated stepwise with the in equation (3.24) and (3.25) defined upper and lower bound. To reduce the complexity in the lower levels, at every node of the tree the later defined partially fixed-/float baseline solution is calculated and the estimate is checked with the a priory knowledge of the baseline. One branch is dropped if the baseline constrains are not fulfilled in a way which is later described. First we would like to mention the partially fixed-/float baseline solution as it had been introduced by the authors of [6][7]. The partially fixed-/float baseline solution should be understood as the unconstrained minimization problem. Instead of the spherical baseline parameters the authors decided to estimate the baseline parameters in the position domain to have a linear model. It is obvious that this is a reasonable choice due to the reduction of the complexity.

Partially fixed-/float means that one set of ambiguities $\check{\boldsymbol{z}}_{\mathbf{1}j_{1,\ldots,k}} = [\check{N}_{j_1}, \ldots, \check{N}_{j_k}]^T$ is fixed to integers dependent on the current node of the tree and the remaining unfixed integers $\boldsymbol{z}_{\mathbf{2}j_{1,\ldots,k}} = [\check{N}_{j_k+1}, \ldots, \check{N}_{j_K}]^T$ which are treated as float parameters and being estimated with the baseline parameters in the following way. Please note that the notation has been changed in relation to the original in [7]:

$$\boldsymbol{z}_{j_{1,\ldots,k}} = \boldsymbol{P}^k \check{\boldsymbol{z}}_{\mathbf{1}j_{1,\ldots,k}} + \bar{\boldsymbol{P}}^k \boldsymbol{z}_{\mathbf{2}j_{1,\ldots,k}} \tag{3.26}$$

The selection matrices are defined as follows:

$$\boldsymbol{P}^k = \begin{bmatrix} \mathbf{1}^{k\times k} \\ \mathbf{0}^{(K-k)\times k} \end{bmatrix} \qquad \bar{\boldsymbol{P}}^k = \begin{bmatrix} \mathbf{0}^{k\times(K-k)} \\ \mathbf{1}^{(K-k)\times(K-k)} \end{bmatrix} \tag{3.27}$$

Now we can formulate the partially float/- fixed minimization problem as:

$$\begin{bmatrix} \check{\hat{\boldsymbol{\xi}}}_{j_{1,\ldots,k}} \\ \boldsymbol{z}_{\mathbf{2}j_{1,\ldots,k}} \end{bmatrix} = \arg \min_{\boldsymbol{\xi}_{j_{1,\ldots,k}}, \boldsymbol{z}_{\mathbf{2}j_{1,\ldots,k}}} \|(\boldsymbol{\Psi} - \boldsymbol{A}\boldsymbol{P}^k \check{\boldsymbol{z}}_{\mathbf{1}j_{1,\ldots,k}}) - \boldsymbol{H}\boldsymbol{\xi}_{j_{1,\ldots,k}} - \boldsymbol{A}\bar{\boldsymbol{P}}^k \boldsymbol{z}_{\mathbf{2}j_{1,\ldots,k}}\|_{\boldsymbol{\Sigma}^{-1}} \tag{3.28}$$

$$\begin{bmatrix} \check{\hat{\boldsymbol{\xi}}}_{j_{1,\ldots,k}} \\ \boldsymbol{z}_{\mathbf{2}j_{1,\ldots,k}} \end{bmatrix} = \left([\boldsymbol{H}\boldsymbol{A}\bar{\boldsymbol{P}}^{\boldsymbol{k}}]^T \boldsymbol{\Sigma}^{-1} [\boldsymbol{H}\boldsymbol{A}\bar{\boldsymbol{P}}^{\boldsymbol{k}}]\right)^{-1} [\boldsymbol{H}\boldsymbol{A}\bar{\boldsymbol{P}}^{\boldsymbol{k}}]^T \boldsymbol{\Sigma}^{-1} \left(\boldsymbol{\Psi} - \boldsymbol{A}\boldsymbol{P}^k \check{\boldsymbol{z}}_{\mathbf{1}j_{1,\ldots,k}}\right) \tag{3.29}$$

$$\tag{3.30}$$

If we have calculated the estimate for the current node, we have to check, if the baseline estimate fulfills our a priori knowledge. Therefore we have to estimate the spherical baseline parameters and their uncertainty. The former step is simply done by the next equations:

$$\check{l}_{j_{1,\ldots,k}} = \|\check{\hat{\boldsymbol{\xi}}}_{j_{1,\ldots,k}}\| \tag{3.31}$$

$$\check{\nu}_{1j_{1,\ldots,k}} = \arctan\left(\frac{\check{\hat{\boldsymbol{\xi}}}_{\boldsymbol{z}j_{1,\ldots,k}}}{\|\check{\hat{\boldsymbol{\xi}}}_{j_{1,\ldots,k}}\|}\right) \tag{3.32}$$

$$\check{\nu}_{2j_{1,\ldots,k}} = \arctan\left(\frac{\check{\hat{\boldsymbol{\xi}}}_{\boldsymbol{y}j_{1,\ldots,k}}}{\check{\hat{\boldsymbol{\xi}}}_{\boldsymbol{x}j_{1,\ldots,k}}}\right) \tag{3.33}$$

More challenging is the derivation of the uncertainty of these parameters because only the length could be assumed to be Gaussian distributed. The authors in [7] suggested to derive the parameters for $\check{\nu}_{1j_{1,\ldots,k}}$ and $\check{\nu}_{2j_{1,\ldots,k}}$ by a Monte-Carlo simulation and store the obtained values in a look-up table for real time applications. This is a big disadvantage of this approach which could lead to reduced performance of the algorithm. Further it should be mentioned that there is no possibility to account for the correlation between the different components of the estimated baseline vector.

$$\boldsymbol{\Sigma}^k_{\begin{bmatrix} \check{\hat{\boldsymbol{\xi}}} \\ \boldsymbol{z}_{\mathbf{2}} \end{bmatrix}} = \left([\boldsymbol{H}\boldsymbol{A}\bar{\boldsymbol{P}}^{\boldsymbol{k}}]^T \boldsymbol{\Sigma}^{-1} [\boldsymbol{H}\boldsymbol{A}\bar{\boldsymbol{P}}^{\boldsymbol{k}}]\right)^{-1} = \begin{bmatrix} \boldsymbol{\Sigma}^k_{\check{\hat{\boldsymbol{\xi}}}} & \boldsymbol{\Sigma}^k_{\check{\hat{\boldsymbol{\xi}}}\boldsymbol{z}_{\mathbf{2}}} \\ \boldsymbol{\Sigma}^k_{\boldsymbol{z}_{\mathbf{2}}\check{\hat{\boldsymbol{\xi}}}} & \boldsymbol{\Sigma}^k_{\boldsymbol{z}_{\mathbf{2}}} \end{bmatrix} \tag{3.34}$$

$$\sigma_{\check{l}^k} = \sqrt{\mathrm{trace}(\boldsymbol{\Sigma}^k_{\check{\hat{\boldsymbol{\xi}}}})} \tag{3.35}$$

Apart from this disadvantage the authors define the acceptance criteria in the following way:

$$|\check{\hat{l}}_{j_{1,\ldots,k}} - \bar{l}| \leq \mu_l \cdot \sigma_{\check{l}^k} \tag{3.36}$$

$$|\check{\hat{\nu}}_{1j_{1,\ldots,k}} - \bar{\nu}_1| \leq \mu_{\nu_1} \cdot \sigma_{\check{\nu}_1^k} \tag{3.37}$$

$$|\check{\hat{\nu}}_{2j_{1,\ldots,k}} - \bar{\nu}_2| \leq \mu_{\nu_2} \cdot \sigma_{\check{\nu}_2^k} \tag{3.38}$$

If finally the algorithm has gone through the tree and there is more than one integer vector left, that one with the lowest value of $\boldsymbol{J}(\boldsymbol{\Psi}, \check{\nu}_1, \check{\nu}_2, \check{l}, \check{\boldsymbol{N}})$ should be chosen.

3.3 Soft Constrained Ambiguity Resolution - Position Domain A Priori Knowledge

3.3.1 Maximum A Posteriori Probability Estimator

The method new developed in this section assumes the a priori knowledge in the Cartesian position domain instead of the current method which assumes the a priori knowledge in the spherical domain. The advantages of this approach, will be derived in this section. The minimization does't contain the non-linear transformation as before and the constrained integer search can be performed without the need of look-up tables as storage of uncertainty parameters predetermined with Monte-Carlo simulations. Again our start point is the MAP estimator, which in this case maximizes the probability of $\boldsymbol{\xi}$ instead of the baseline parameters in the spherical domain, if a measurement $\boldsymbol{\Psi}$ is given. We use the rule of Bayes, the assumption of independent statistical a priori knowledge of $\boldsymbol{\xi}$ and $\boldsymbol{N}$. The noise statistics again assumed to be Gaussian but with the important difference that our model is linear; compare equations (3.14) and (3.40):

$$\max_{\boldsymbol{\xi},\boldsymbol{N}} p(\boldsymbol{\xi},\boldsymbol{N}|\boldsymbol{\Psi}) = \max_{\boldsymbol{\xi},\boldsymbol{N}} p(\boldsymbol{\Psi}|\boldsymbol{\xi},\boldsymbol{N}) \cdot \frac{p(\boldsymbol{\xi})p(\boldsymbol{N})}{p(\boldsymbol{\Psi})} \tag{3.39}$$

$$p(\boldsymbol{\Psi}|\boldsymbol{\xi},\boldsymbol{N}) = \frac{1}{\sqrt{(2\pi)^p|\boldsymbol{\Sigma}|}} \exp\Big(-\frac{1}{2}\|\boldsymbol{\Psi}-\boldsymbol{H}\boldsymbol{\xi}-\boldsymbol{A}\boldsymbol{N}\|^2_{\boldsymbol{\Sigma}^{-1}}\Big) \tag{3.40}$$

Further an important difference is now the a priori knowledge in the position domain. At this point we want to emphasize that this a priori knowledge does not have to be decorrelated, rather the normal case will be that the a priori knowledge is correlated and therefore $\boldsymbol{\Sigma}_{\bar{\xi}}$ will have not only diagonal elements greater zero. This a priory knowledge could come e.g. from a state-space model dependent on the dynamics of the object. Like before the variables with a bar like now $\bar{\boldsymbol{\xi}}$ denote the true values.

$$p(\boldsymbol{\xi}) = \frac{1}{\sqrt{(2\pi)^3|\boldsymbol{\Sigma}_{\bar{\xi}}|}} \exp\Big(-\frac{1}{2}\|\boldsymbol{\xi}-\bar{\boldsymbol{\xi}}\|^2_{\boldsymbol{\Sigma}_{\bar{\xi}}^{-1}}\Big) \tag{3.41}$$

As in the current case we don't have any a priori knowledge about the ambiguities $\boldsymbol{N}$ therefore the same equal distribution as defined in (3.17) applies to this case. Also the orthogonal decomposition could be done in the same way as before, just the additional constrains are different. We obtain the following minimization problem. Note that we define $\check{\boldsymbol{\xi}}(\boldsymbol{N})$ in the same way as for the other methods:

$$\begin{aligned}
&\min_{\boldsymbol{\xi},\boldsymbol{N}} \boldsymbol{J}(\boldsymbol{\xi},\boldsymbol{N}) \\
&:= \min_{\boldsymbol{\xi},\boldsymbol{N}} \Big(\|\boldsymbol{\Psi}-\boldsymbol{H}\boldsymbol{\xi}-\boldsymbol{A}\boldsymbol{N}\|^2_{\boldsymbol{\Sigma}^{-1}} + \|\boldsymbol{\xi}-\bar{\boldsymbol{\xi}}\|^2_{\boldsymbol{\Sigma}_{\bar{\xi}}^{-1}}\Big) \qquad (3.42)\\
&= \min_{\boldsymbol{N}} \Big(\|\hat{\boldsymbol{N}}-\boldsymbol{N}\|^2_{\boldsymbol{\Sigma}^{-1}_{\hat{N}}} + \min_{\boldsymbol{\xi},} \Big(\|\boldsymbol{P}_H(\boldsymbol{\Psi}-\boldsymbol{A}\boldsymbol{N}) - \boldsymbol{H}\boldsymbol{\xi}\|^2_{\boldsymbol{\Sigma}^{-1}} + \|\boldsymbol{\xi}-\bar{\boldsymbol{\xi}}\|^2_{\boldsymbol{\Sigma}_{\bar{\xi}}^{-1}}\Big)\Big) \\
&= \min_{\boldsymbol{N}} \Big(\|\hat{\boldsymbol{N}}-\boldsymbol{N}\|^2_{\boldsymbol{\Sigma}^{-1}_{\hat{N}}} + \min_{\boldsymbol{\xi},} \Big(\|\boldsymbol{H}\underbrace{(\boldsymbol{H}^T\boldsymbol{\Sigma}^{-1}\boldsymbol{H})^{-1}\boldsymbol{H}^T\boldsymbol{\Sigma}^{-1}(\boldsymbol{\Psi}-\boldsymbol{A}\boldsymbol{N})}_{=:\check{\boldsymbol{\xi}}(\boldsymbol{N})} - \boldsymbol{H}\boldsymbol{\xi}\|^2_{\boldsymbol{\Sigma}^{-1}} + \|\boldsymbol{\xi}-\bar{\boldsymbol{\xi}}\|^2_{\boldsymbol{\Sigma}_{\bar{\xi}}^{-1}}\Big)\Big) \\
&= \min_{\boldsymbol{N}} \Big(\|\hat{\boldsymbol{N}}-\boldsymbol{N}\|^2_{\boldsymbol{\Sigma}^{-1}_{\hat{N}}} + \min_{\boldsymbol{\xi},} \Big(\|\check{\boldsymbol{\xi}}(\boldsymbol{N})-\boldsymbol{\xi}\|^2_{\boldsymbol{\Sigma}^{-1}_{\check{\xi}(\boldsymbol{N})}} + \|\boldsymbol{\xi}-\bar{\boldsymbol{\xi}}\|^2_{\boldsymbol{\Sigma}_{\bar{\xi}}^{-1}}\Big)\Big) \qquad (3.43)
\end{aligned}$$

The variance/-covariance matrix is: $\boldsymbol{\Sigma}^{-1}_{\check{\xi}(\boldsymbol{N})} := (\boldsymbol{H}^T\boldsymbol{\Sigma}^{-1}\boldsymbol{H})^{-1}$

Let us compare this result with the minimizer of the current method (3.20). Like all constrained methods the minimization cannot be separated. The minimization problem in (3.43) could be solved with a similar tree search as the current method refer to subsection 3.2.2. Recall that at every path note in the tree, the current method evaluates the unconstrained solution due to the non-linear constrains in the problem. But we can see with the following derivation, that it is possible to determine the constrained baseline estimate for one fixed integer set in a closed form. This is notated as $\check{\boldsymbol{\xi}}_{MAP}(\boldsymbol{N})$:

$$\check{\boldsymbol{\xi}}_{MAP}(\boldsymbol{N}) := \arg\min_{\boldsymbol{\xi},} \left(\|\check{\boldsymbol{\xi}}(\boldsymbol{N}) - \boldsymbol{\xi}\|^2_{\boldsymbol{\Sigma}^{-1}_{\check{\boldsymbol{\xi}}(\boldsymbol{N})}} + \|\boldsymbol{\xi} - \bar{\boldsymbol{\xi}}\|^2_{\boldsymbol{\Sigma}_{\bar{\boldsymbol{\xi}}}{}^{-1}} \right) \tag{3.44}$$

$$\begin{aligned} C(\boldsymbol{\xi}, \boldsymbol{N}) &:= \|\check{\boldsymbol{\xi}}(\boldsymbol{N}) - \boldsymbol{\xi}\|^2_{\boldsymbol{\Sigma}^{-1}_{\check{\boldsymbol{\xi}}(\boldsymbol{N})}} + \|\boldsymbol{\xi} - \bar{\boldsymbol{\xi}}\|^2_{\boldsymbol{\Sigma}_{\bar{\boldsymbol{\xi}}}{}^{-1}} \\ &= (\check{\boldsymbol{\xi}}(\boldsymbol{N}) - \boldsymbol{\xi})^T \boldsymbol{\Sigma}^{-1}_{\check{\boldsymbol{\xi}}(\boldsymbol{N})} (\check{\boldsymbol{\xi}}(\boldsymbol{N}) - \boldsymbol{\xi}) + (\boldsymbol{\xi} - \bar{\boldsymbol{\xi}})^T \boldsymbol{\Sigma}_{\bar{\boldsymbol{\xi}}}{}^{-1} (\boldsymbol{\xi} - \bar{\boldsymbol{\xi}}) \end{aligned}$$

$$\begin{aligned} \mathbf{0} &= \frac{\partial}{\partial \boldsymbol{\xi}} C(\boldsymbol{\xi}, \boldsymbol{N}) \\ \mathbf{0} &= -2\boldsymbol{\Sigma}_{\bar{\boldsymbol{\xi}}}{}^{-1} \check{\boldsymbol{\xi}}(\boldsymbol{N}) + 2\boldsymbol{\Sigma}_{\bar{\boldsymbol{\xi}}}{}^{-1} \boldsymbol{\xi} + 2\boldsymbol{\Sigma}_{\bar{\boldsymbol{\xi}}}{}^{-1} \boldsymbol{\xi} - 2(\bar{\boldsymbol{\xi}}^T \boldsymbol{\Sigma}_{\bar{\boldsymbol{\xi}}}{}^{-1})^T \end{aligned}$$

$$\check{\boldsymbol{\xi}}_{MAP}(\boldsymbol{N}) = (\boldsymbol{\Sigma}^{-1}_{\check{\boldsymbol{\xi}}(\boldsymbol{N})} + \boldsymbol{\Sigma}_{\bar{\boldsymbol{\xi}}}{}^{-1})^{-1} (\boldsymbol{\Sigma}^{-1}_{\check{\boldsymbol{\xi}}(\boldsymbol{N})} \check{\boldsymbol{\xi}}(\boldsymbol{N}) + \boldsymbol{\Sigma}_{\bar{\boldsymbol{\xi}}}{}^{-1} \bar{\boldsymbol{\xi}}) \tag{3.45}$$

With all that information we could introduce the new developed constrained integer tree search in the next section.

3.3.2 Constrained Integer Search

The current tree search algorithm developed by Henkel and Jurkowski has the disadvantage that the transformation of the uncertainty parameters from the spherical to the position domain during the search is rarely possible. With the a priori knowledge in the position domain directly, we derive a constrained integer search method which does not have this problem. This new developed algorithm differs from the current method mainly in two aspects. The first aspect is the different minimization problem evaluated at every path note and the second one is the different acceptance criteria to evaluate the estimate obtained from the first step. The notation of subsection 3.2.2 applies for this subsection in the same way, and is not mentioned again. Further the determination of the upper end lower bounds to construct the search tree step by step at every note is done in the same way. With the help of the bootstrapping solution $\hat{N}^{l}_{j_l|j_{1,\dots,l-1}}$ and the obtained variances of the bootstrapping solution $\sigma^2_{\hat{N}_{l|1,\dots,l-1}}$ as well as the initially selected size of the search space χ^2 the upper and lower bound has been defined in (3.24) and (3.25) as below:

$$u_{\hat{N}^k_{j_k}} = \hat{N}^k_{j_k|j_{1,\dots,k-1}} - \sigma_{\hat{N}_k|j_{1,\dots,k-1}} \sqrt{\chi^2 - \sum_{l=1}^{k-1} \frac{\left(\hat{N}^l_{j_l} - \hat{N}^l_{j_l|j_{1,\dots,l-1}}\right)^2}{\sigma^2_{\hat{N}_{l|1,\dots,l-1}}}}$$

$$o_{\hat{N}^k_{j_k}} = \hat{N}^k_{j_k|j_{1,\dots,k-1}} + \sigma_{\hat{N}_k|j_{1,\dots,k-1}} \sqrt{\chi^2 - \sum_{l=1}^{k-1} \frac{\left(\hat{N}^l_{j_l} - \hat{N}^l_{j_l|j_{1,\dots,l-1}}\right)^2}{\sigma^2_{\hat{N}_{l|1,\dots,l-1}}}}$$

Then at every node of the current level k the **constrained** partially fixed/-float baseline solution is translated from equation (3.45) in the following way:

$$\boldsymbol{z}_{j_{1,\dots,k}} = \boldsymbol{P}^k \check{\boldsymbol{z}}_{\mathbf{1}j_{1,\dots,k}} + \bar{\boldsymbol{P}}^k \boldsymbol{z}_{\mathbf{2}j_{1,\dots,k}}$$

The selection matrices are defined as follows:

$$\boldsymbol{P}^k = \begin{bmatrix} \mathbf{1}^{k\times k} \\ \mathbf{0}^{(K-k)\times k} \end{bmatrix} \qquad \bar{\boldsymbol{P}}^k = \begin{bmatrix} \mathbf{0}^{k\times(K-k)} \\ \mathbf{1}^{(K-k)\times(K-k)} \end{bmatrix} \tag{3.46}$$

The variables defined in the previous section change to the variables for the **constrained** partially fixed/-float baseline solution in the following way:

$$\check{\boldsymbol{\xi}}(\boldsymbol{N}) \rightarrow \check{\hat{\boldsymbol{\xi}}}(\check{\boldsymbol{z}}_{\mathbf{1}j_{1,\dots,k}}) := \check{\hat{\boldsymbol{\xi}}}_{j_{1,\dots,k}} \tag{3.47}$$

$$\check{\boldsymbol{\xi}}_{\mathrm{MAP}}(\boldsymbol{N}) \rightarrow \check{\boldsymbol{\xi}}_{\mathrm{MAP}}(\check{\boldsymbol{z}}_{\mathbf{1}j_{1,\dots,k}}) := \check{\hat{\boldsymbol{\xi}}}_{\mathrm{MAP},j_{1,\dots,k}} \tag{3.48}$$

With this relationship we can formulate the **constrained** partially float/- fixed minimization problem.

$$\begin{bmatrix} \check{\hat{\boldsymbol{\xi}}}_{j_{1,\dots,k}} \\ \boldsymbol{z}_{\mathbf{2}j_{1,\dots,k}} \end{bmatrix} = \left([\boldsymbol{HA}\bar{\boldsymbol{P}}^{\boldsymbol{k}}]^T \boldsymbol{\Sigma}^{-1} [\boldsymbol{HA}\bar{\boldsymbol{P}}^{\boldsymbol{k}}]\right)^{-1} [\boldsymbol{HA}\bar{\boldsymbol{P}}^{\boldsymbol{k}}]^T \boldsymbol{\Sigma}^{-1} \left(\boldsymbol{\Psi} - \boldsymbol{AP}^k \check{\boldsymbol{z}}_{\mathbf{1}j_{1,\dots,k}}\right)$$

$$\check{\hat{\boldsymbol{\xi}}}_{MAP,j_{1,\dots,k}} = \arg\min_{\boldsymbol{\xi},} \left(\|\check{\hat{\boldsymbol{\xi}}}_{j_{1,\dots,k}} - \boldsymbol{\xi}\|^2_{\boldsymbol{\Sigma}^{-1}_{\check{\boldsymbol{\xi}}(\boldsymbol{N})}} + \|\boldsymbol{\xi} - \bar{\boldsymbol{\xi}}\|^2_{\boldsymbol{\Sigma}_{\bar{\boldsymbol{\xi}}}{}^{-1}} \right) \tag{3.49}$$

$$= (\boldsymbol{\Sigma}^{-1}_{\check{\boldsymbol{\xi}}(\boldsymbol{N})} + \boldsymbol{\Sigma}_{\bar{\boldsymbol{\xi}}}{}^{-1})^{-1} (\boldsymbol{\Sigma}^{-1}_{\check{\boldsymbol{\xi}}(\boldsymbol{N})} \check{\hat{\boldsymbol{\xi}}}_{j_{1,\dots,k}} + \boldsymbol{\Sigma}_{\bar{\boldsymbol{\xi}}}{}^{-1} \bar{\boldsymbol{\xi}}) \tag{3.50}$$

The variance-/covariance matrix is shown in the following equation. Please note that we have dropped the index for the dependency to the path in the tree for better readability:

$$\boldsymbol{\Sigma}_{\check{\hat{\boldsymbol{\xi}}}_{\text{MAP}}} = (\boldsymbol{\Sigma}^{-1}_{\check{\hat{\boldsymbol{\xi}}}(\boldsymbol{N})} + \boldsymbol{\Sigma}_{\bar{\boldsymbol{\xi}}}{}^{-1})^{-1} \tag{3.51}$$

When we have calculated the estimate $\check{\hat{\boldsymbol{\xi}}}_{MAP,j_{1,\ldots,k}}$ for the current node, we have to check if the baseline estimate fulfills our a priori knowledge. We introduce a method which doesn't need the non-linear transformation to the spherical domain, because the a priori knowledge and the estimate are both in the position domain. We suggest to select the acceptance area, depending on a user defined probability bound P_{F}. With that probability P_{F} an integer set at the current note doesn't fulfill the a priori knowledge and is therefore rejected by the test. The opposite event, that an integer set fulfills the a priori knowledge is then defined as $P_{\text{accept}} = 1 - P_{\text{F}}$. For the acceptance criteria that means: the estimate $\check{\hat{\boldsymbol{\xi}}}_{MAP,j_{1,\ldots,k}}$ has to fulfill the a priori knowledge with the probability P_{accept}. For the acceptance criteria that means:

$$\|\check{\hat{\boldsymbol{\xi}}}_{\text{MAP},j_{1,\ldots,k}} - \bar{\boldsymbol{\xi}}\|^2_{\boldsymbol{\Sigma}^{-1}_{\text{Check}}} \leq c \qquad \text{for} \quad P_{\text{accept}} = P(\|\check{\hat{\boldsymbol{\xi}}}_{\text{MAP},j_{1,\ldots,k}} - \bar{\boldsymbol{\xi}}\|^2_{\boldsymbol{\Sigma}^{-1}_{\text{Check}}} \leq c) \tag{3.52}$$

That leads us to the questions: How could the probabilities of $P(\|\check{\hat{\boldsymbol{\xi}}}_{\text{MAP},j_{1,\ldots,k}} - \bar{\boldsymbol{\xi}}\|^2_{\boldsymbol{\Sigma}^{-1}_{\text{Check}}})$ be described and how has the matrix $\boldsymbol{\Sigma}^{-1}_{\text{Check}}$ to be defined? The answers to these questions will be discussed now.To derive the distribution we first look at the distributions of the individual terms in the acceptance criteria:

$$p_{\check{\hat{\boldsymbol{\xi}}}_{\text{MAP}}}(\boldsymbol{\xi}) = \frac{1}{\sqrt{(2\pi)^3|\boldsymbol{\Sigma}_{\check{\hat{\boldsymbol{\xi}}}_{\text{MAP}}}|}} \exp\Big(-\frac{1}{2}\|\boldsymbol{\xi} - \bar{\boldsymbol{\xi}}\|^2_{\boldsymbol{\Sigma}^{-1}_{\check{\hat{\boldsymbol{\xi}}}_{\text{MAP}}}}\Big) \tag{3.53}$$

$$p_{\bar{\boldsymbol{\xi}}}(\boldsymbol{\xi}) = \frac{1}{\sqrt{(2\pi)^3|\boldsymbol{\Sigma}_{\bar{\boldsymbol{\xi}}}|}} \exp\Big(-\frac{1}{2}\|\boldsymbol{\xi} - \bar{\boldsymbol{\xi}}\|^2_{\boldsymbol{\Sigma}_{\bar{\boldsymbol{\xi}}}{}^{-1}}\Big) \tag{3.54}$$

Both the random variables are described with multivariate Gaussian distributions around the true value. The difference of these two random variables is again Gaussian distributed but around zero.

$$p_{\check{\hat{\boldsymbol{\xi}}}-\bar{\boldsymbol{\xi}}}(\boldsymbol{\xi}) = \frac{1}{\sqrt{(2\pi)^3|\boldsymbol{\Sigma}_{\bar{\boldsymbol{\xi}}} + \boldsymbol{\Sigma}_{\check{\hat{\boldsymbol{\xi}}}_{\text{MAP}}}|}} \exp\Big(-\frac{1}{2}\|\boldsymbol{\xi}\|^2_{(\boldsymbol{\Sigma}_{\bar{\boldsymbol{\xi}}}+\boldsymbol{\Sigma}_{\check{\hat{\boldsymbol{\xi}}}_{\text{MAP}}})^{-1}}\Big) \tag{3.55}$$

Now we have to find a transformation with which we obtain decorrelated normal distributed random variables. Therefore we use the Cholesky decomposition of the variance-/covariance matrix. This is possible because it is a symmetrical and positive definite matrix; see appendix (A1):

$$\boldsymbol{\Sigma}^{-1}_{\text{Check}} := \boldsymbol{\Sigma}_{\bar{\boldsymbol{\xi}}} + \boldsymbol{\Sigma}_{\check{\hat{\boldsymbol{\xi}}}_{\text{MAP}}} \tag{3.56}$$

$$\boldsymbol{\Sigma}^{-1}_{\text{Check}} = \boldsymbol{G}\boldsymbol{G}^T \tag{3.57}$$

We define now the transformation of the random variables with the help of the decomposed variance/-covariance matrix and develop the resulted acceptance criteria:

$$\boldsymbol{\varepsilon}_{j_{1,\ldots,k}} := \boldsymbol{G}^T\big(\check{\hat{\boldsymbol{\xi}}}_{\text{MAP},j_{1,\ldots,k}} - \bar{\boldsymbol{\xi}}\big) \quad \rightarrow \quad \big(\check{\hat{\boldsymbol{\xi}}}_{\text{MAP},j_{1,\ldots,k}} - \bar{\boldsymbol{\xi}}\big) = (\boldsymbol{G}^T)^{-1}\boldsymbol{\varepsilon}_{j_{1,\ldots,k}} \tag{3.58}$$

$$
\begin{aligned}
\|\check{\hat{\boldsymbol{\xi}}}_{\text{MAP},j_{1,\dots,k}} - \bar{\boldsymbol{\xi}}\|^2_{\boldsymbol{\Sigma}^{-1}_{\text{Check}}} &\leq c \\
\|(\boldsymbol{G}^T)^{-1}\boldsymbol{\varepsilon}_{j_{1,\dots,k}}\|^2_{\boldsymbol{\Sigma}^{-1}_{\text{Check}}} &\leq c \\
\left((\boldsymbol{G}^T)^{-1}\boldsymbol{\varepsilon}_{j_{1,\dots,k}}\right)^T \boldsymbol{\Sigma}^{-1}_{\text{Check}}(\boldsymbol{G}^T)^{-1}\boldsymbol{\varepsilon}_{j_{1,\dots,k}} &\leq c \\
\boldsymbol{\varepsilon}^T_{j_{1,\dots,k}} \underbrace{\boldsymbol{G}^{-1}\boldsymbol{G}\boldsymbol{G}^T(\boldsymbol{G}^T)^{-1}}_{=\boldsymbol{I}} \boldsymbol{\varepsilon}_{j_{1,\dots,k}} &\leq c \\
\boldsymbol{\varepsilon}^T_{j_{1,\dots,k}}\boldsymbol{\varepsilon}_{j_{1,\dots,k}} &\leq c
\end{aligned}
\tag{3.59}
$$

The obtained formulation of the acceptance criteria is now a squared sum of normal Gaussian distributed variables and that's why the distribution is obtained by the Chi-squared distribution; see appendix (A2). In this case the dimension of the χ^2 distribution is three, due to the three components of the baseline estimate $\check{\hat{\boldsymbol{\xi}}}_{\text{MAP},j_{1,\dots,k}}$.

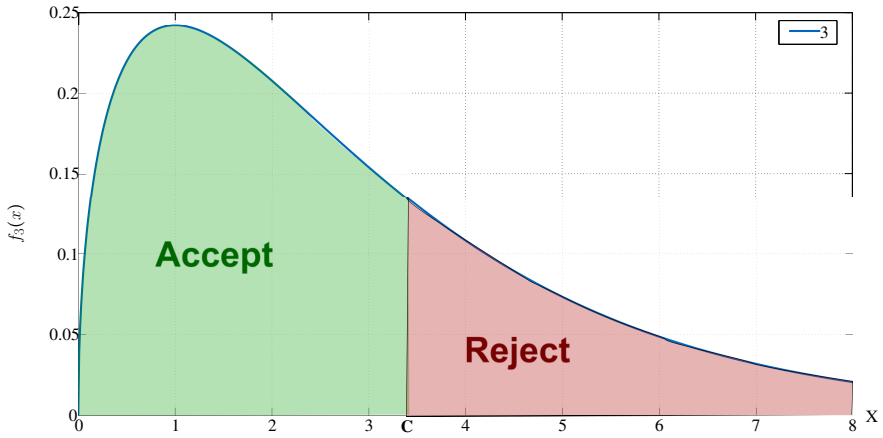

Figure 3.2: PDF of the Chi-squared distribution with dimention three χ^2_3.

With the distribution of $(\boldsymbol{\varepsilon}^T_{j_{1,\dots,k}}\boldsymbol{\varepsilon}_{j_{1,\dots,k}})$ we can derive how the bound c has to be chosen that equation (3.52) is fulfilled.

$$
\begin{aligned}
P_{\text{accept}} &= P\left(\|\check{\hat{\boldsymbol{\xi}}}_{\text{MAP},j_{1,\dots,k}} - \bar{\boldsymbol{\xi}}\|^2_{\boldsymbol{\Sigma}^{-1}_{\text{Check}}} \leq c\right) \\
&= P\left(\boldsymbol{\varepsilon}^T_{j_{1,\dots,k}}\boldsymbol{\varepsilon}_{j_{1,\dots,k}} \leq c\right) \\
&= \int_0^c f_3(x)dx
\end{aligned}
\tag{3.60}
$$

This integral has only to be solved once for a given value of P_{accept} because it only depends on the degrees of the distribution. In our case this is every time 3 and due to that, it doesn't increase the complexity of the algorithm.
In the next figure one can see the modified tree search with the steps which has do be done to check at the current note if the integer set should be accepted or rejected.

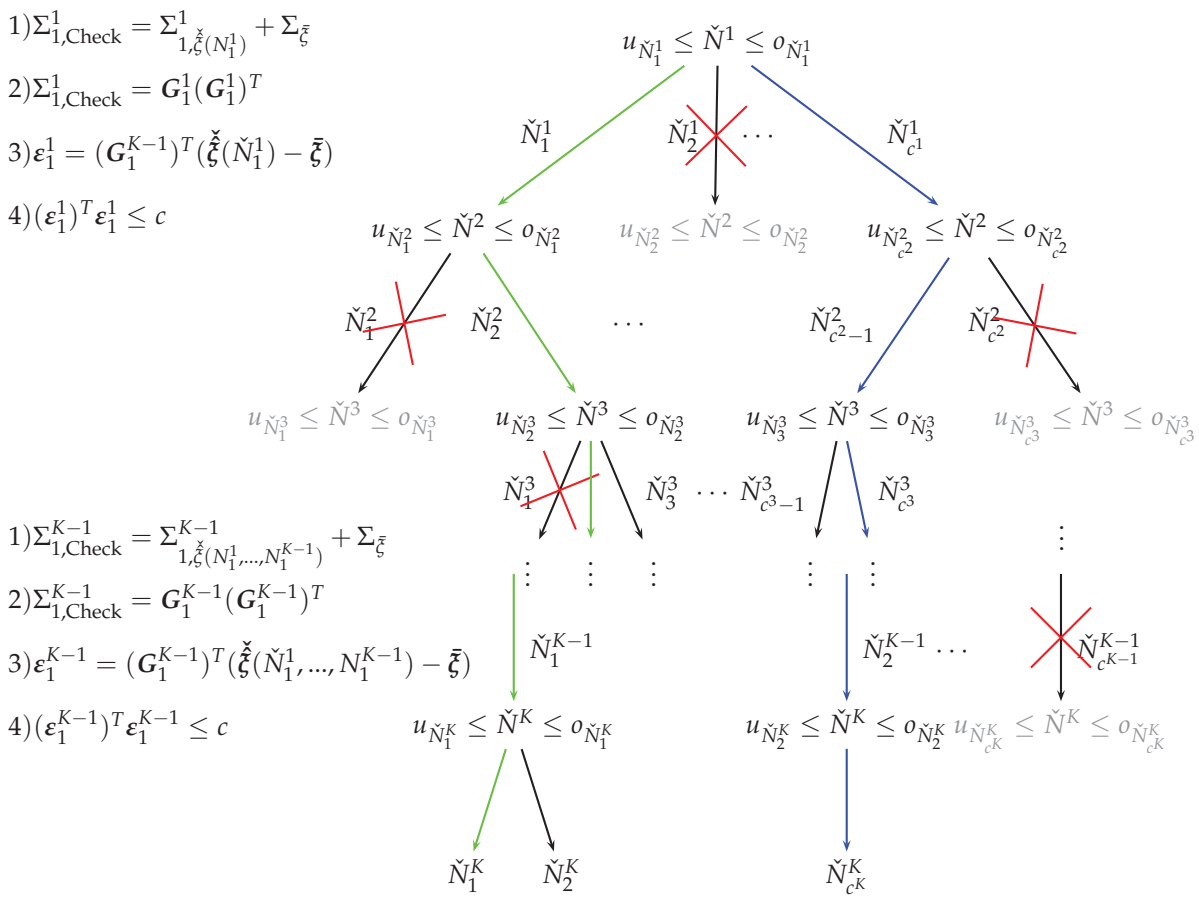

Figure 3.3: Search tree: Fulfillment of the constrains with a user defined failure rate are checked at each path node to reduce the final number of branches.(Figure adapted with permission of Jurkowski P.)

4. Experimental Results

4.1 Receiver Setup

4.1.1 Novatel OEMStar™Receiver

Figure 4.1: Novatel OEMStar Receiver with FlexPak G2

For the measurements during this thesis two Novatel OEMStar™receivers with the FlexPak-G2™have been used. It is a low cost single frequency (L1) receiver for GPS and GLONASS. The receiver can track code and carrier phase measurements from up to 14 satellites with a data rate of maximum 10Hz. The timing accurency is mentioned with 20ns. That is a very important property which a receiver needs to fulfill the 3rd requirement mentioned on page 16. The receiver comes with a reliable enclosure to deliver appropriate interfaces and operation capability suitable for the environmental conditions during the planed experiments. The possibility to adjust the receiver configuration via software commands opens up the possibility to control the receiver and read out of GPS and GLONASS raw data in binary format. Later transformation to Receiver Independent Exchange Format (RINEX) is possible. In the following section the receiver and additional equipment is described in more detail. For reference see [14].

4.1.2 Laptop and Control Software

The Novatel's Control and Display Unit (CDU) software, delivered with the receivers, makes it possible to either control the receiver and to receive log-massages from the receivers. With an ordinary personal computer it is possible to communicate with the receiver via Universal Serial Bus (USB) or Communications Port (COM) interfaces. It is recommended to use the USB interface to have enough transmission rate while logging Global Navigation Satellite System (GNSS) data. During the experiments it was only possible to log 10Hz raw ranging information via the USB interfaces. After logging the data to a gps-file they could be transformed by the software tool Convert4 to the RINEX format. Finally the RINEX files were parsed to MATrix LABoratory (MATLAB) by a modified parser which could handle some specialty like automated parsing of all RINEX files of one measurement and constructs a combined MATLAB file.

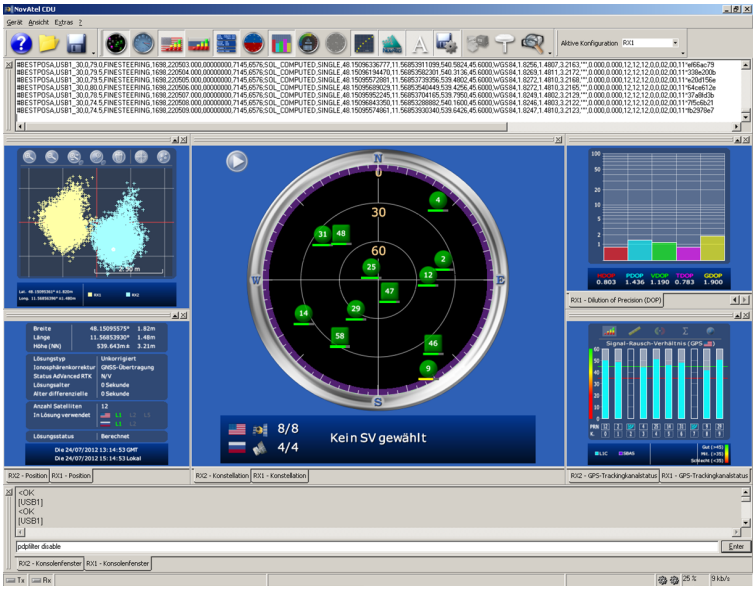

Figure 4.2: Novatel's CDU™software to either control the receiver and to log measurement data.

4.1.3 Antennas

The Novatel OEMStar™receivers can supply power for a Low Noise Amplifier (LNA) contained in an active Antenna via the Coaxial Cable by maintaining the isolation between the Direct Current (DC) power supply and Radio Frequency (RF) signal received by the antenna[14]. Due to that capability it is advantageous to use an active antenna which can compensate the line loss by using an LNA. But some more facts should be considered before choosing the antenna. First the phase center stability is a very important aspect if you do accurate relative carrier phase based positioning or attitude determination. Due to the fact that absolute phase center variations are not interesting for relative positioning only differential phase center variations between different antennas introduce biases and could make ambiguity resolution as integers more challenging. At least for very short base lines one could reduce that effect by using antennas with the same phase center variation characteristics. That is possible because one can assume that the satellite unit vectors for satellite k and receiver $r = \{1, 2\}$ are the same $\vec{e}^k = \vec{e}_1^k \approx \vec{e}_2^k$ and that's why the phase center variations which are a function of the arrival angle of the electromagnetic waves are the same. For longer baselines this assumption is not valid and therefore only accurate antenna models can compensate the additionally introduced biases. In this thesis experiments with short baselines and identical antennas should not require additional antenna models. Second multipath interference could be reduced by choosing an antenna which reduces this influence by its construction. Note that high multipath interference could also influence the phase center stability of the antenna. For this thesis two identical Novatel GNSS Antennas 701GG were used.

4.1.4 Coaxial Cable

To meet the specifications an optimal antenna receiver interconnection is required. Therefore the coaxial cable should match the antenna and receiver impedance for undisturbed signal transmission. In relative carrier phase positioning and attitude determination algorithms like in this thesis different line timing delays introduce unwanted biases if the algorithm does not compensate that effect. In our case we take it into account by using coaxial cables with the same length of 10m.

4.2 Receiver Quality Analysis

4.2.1 Zero Baseline Test

The aim of a zero baseline test, is to verify the performance of a receiver for double-difference carrier phase ambiguity resolution. Recalling equation (2.35):

$$\Delta\nabla\phi_{12}^{kl} = (\vec{e}^{k} - \vec{e}^{l})^{T}\vec{\xi} + \Delta\nabla b_{12}^{kl} + \lambda\Delta\nabla N_{12}^{kl} + \Delta\nabla\epsilon_{12}^{k}$$

One can see that with $\vec{\xi} = \vec{0}$ the first term which contains the satellite movement vanishes. This happens only if the 3rd requirement is fulfilled and therefore the differential receiver time bias is small enough. If in addition to that also the 4th Requirement is fulfilled and no other satellite receiver dependent biases exist i.e. $\Delta\nabla b_{12}^{kl} = 0$, the remaining therms only depend on the integer ambiguity term plus noise. For the definition of the receiver requirements refer to page 16.

$$\Delta\nabla\phi_{12}^{kl} = \lambda\Delta\nabla N_{12}^{kl} + \Delta\nabla\epsilon_{12}^{k}$$

With the 2nd requirement the double difference in the zero baseline case should be constant over the course of time and the 1st requirement says that only exact integer values occur. The following figures 4.3 and 4.4 make clear that all the requirements are perfectly fulfilled by the Novatel OEMStar™receiver.
In Figure 4.3 one can see that the integer terms are in any case an integer and remains constant over the time one satellite is visible. Please note, that some satellites which are available and shown in the legend, hide in the plot behind other satellites, because they have the same integer ambiguity value.

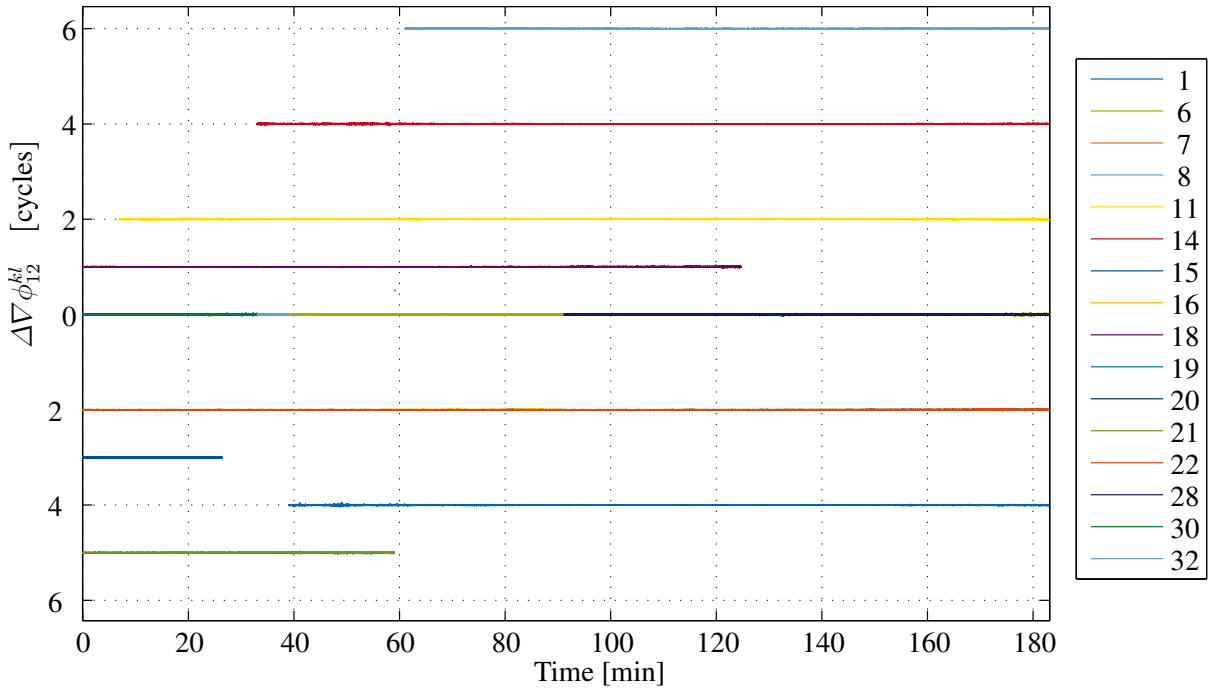

Figure 4.3: Double difference carrier phase measurements of a zero baseline test setup. It shows constant integer double difference values all the time the satellite is visible.

In Figure 4.4 the rounded integer value of the first epoch, when a satellite is visible, is removed that the noise or a possible bias or drift can be seen better. But we see that there is no bias nor any drift visible. With this result we can conclude that the Novatel OEMStar™receiver fulfills all requirements, which we mentioned in chapter 2; see page 16.

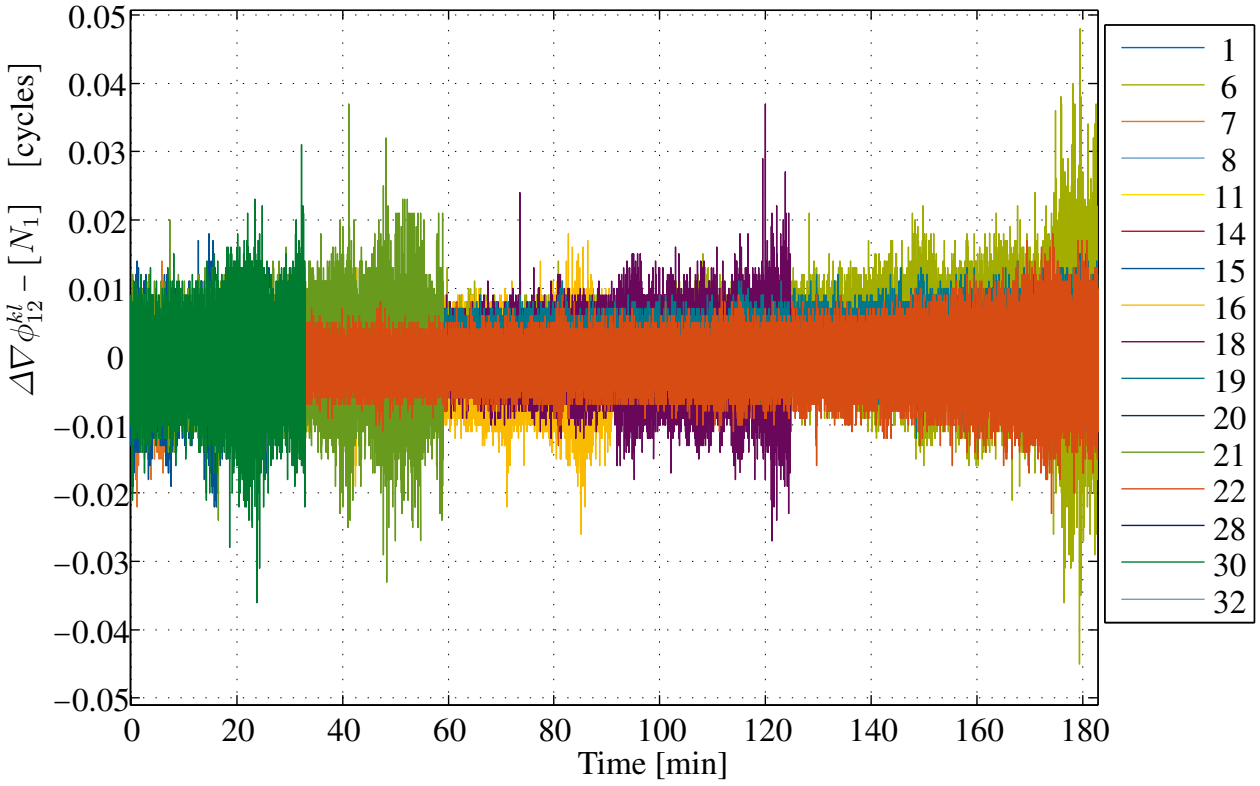

Figure 4.4: Double difference carrier phase measurements of a zero baseline test setup with respect to the rounded integer value of the 1st epoch a satellite is visible denoted as $[N_1]$.

The following figures show a counter example obtained by the Novatel OEMStar™receiver with disabled clock steering in figure 4.5 and 4.6. The receivers have been operating with clock steering enabled until $t = 0$. With the start of measurement recording the clock steering has been switched off. In Figure 4.5 it is visible that at the beginning, due to the enabled clock steering prior $t = 0$, the double difference values are even integers. But over the course time the double differences are drifting and ne

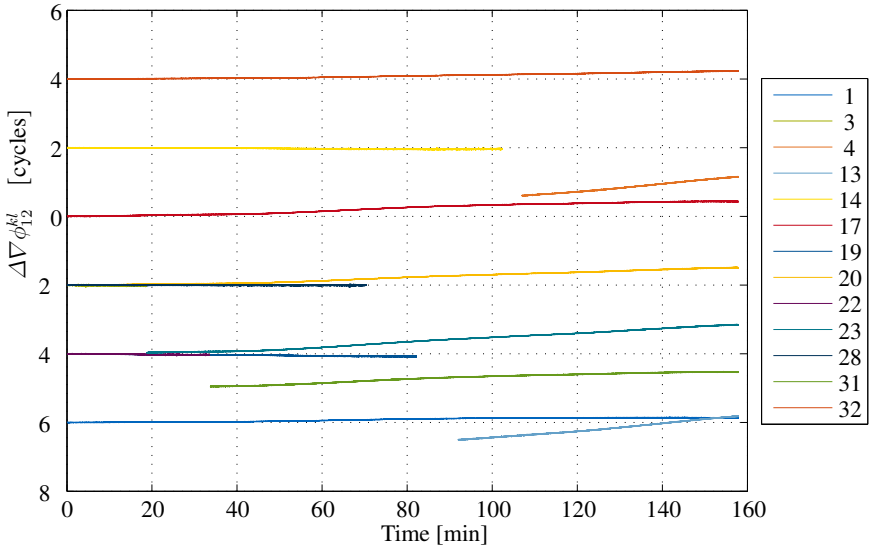

Figure 4.5: Double difference carrier phase measurements of a zero baseline test setup with disabled clock steering.

In Figure 4.6 the rounded integer value of the first epoch, when a satellite is visible, is removed that the noise or a possible bias or drift can be seen better. In this figure it can be seen how the double differences drift gradually. To explain exactly why the double differences change in that way, it is good to have an extra look at the differential clock offset between the receivers. In the next subsection one will see in figure 4.10 the receiver differential clock offset for the same measurement. That will explain the variation in the drift of the double differences, due to variations in the clock drift rates. Further the drift depends on the position of the satellite in relation to the reference

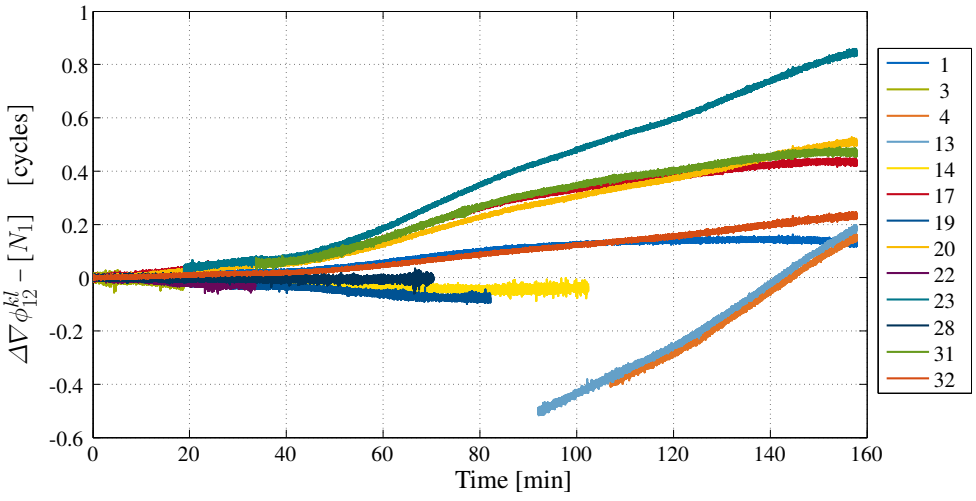

Figure 4.6: Double difference carrier phase measurements of a zero baseline test setup with disabled clock steering and with respect to the rounded integer value of the 1st epoch a satellite is visible denoted as $[N_1]$.

4.2.2 Receiver Clock Errors

From the previous section we know that the Novatel OEMStar™receiver fulfills all requirements. Therefore we expect the clock offsets to be very small. In figure 4.7 we see the receiver clock offsets $\delta\tau_r$ for receiver one and two. As expected the clock offsets are very small. We would like to note that the y-axis is scaled with 10^{-8}. Figure 4.8 shows the difference between the receiver clock offsets $\Delta\delta\tau_{12}$ which is mainly interesting for double difference measurements like used in this thesis. That can be traced back to the fact that absolute variations in the receiver clocks don't introduce errors to double differences, mainly relative clock offsets $\Delta\tau_{12}$ would introduce errors in the estimated satellite position. In that case the 3rd requirement is not fulfilled, because the estimate of the satellite unit vectors would be different. Additional it is interesting to note that the differential clock error is even smaller due to the fact that both receivers sear the receiver clocks in the same way.

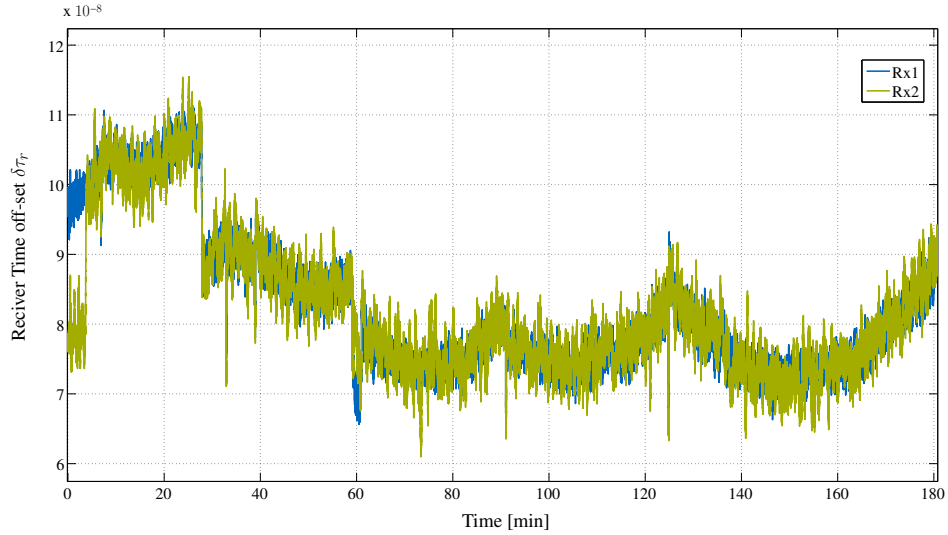

Figure 4.7: Receiver time offsets $\delta\tau_r$ of the Novatel OEMStar™receiver with disabled clock steering.

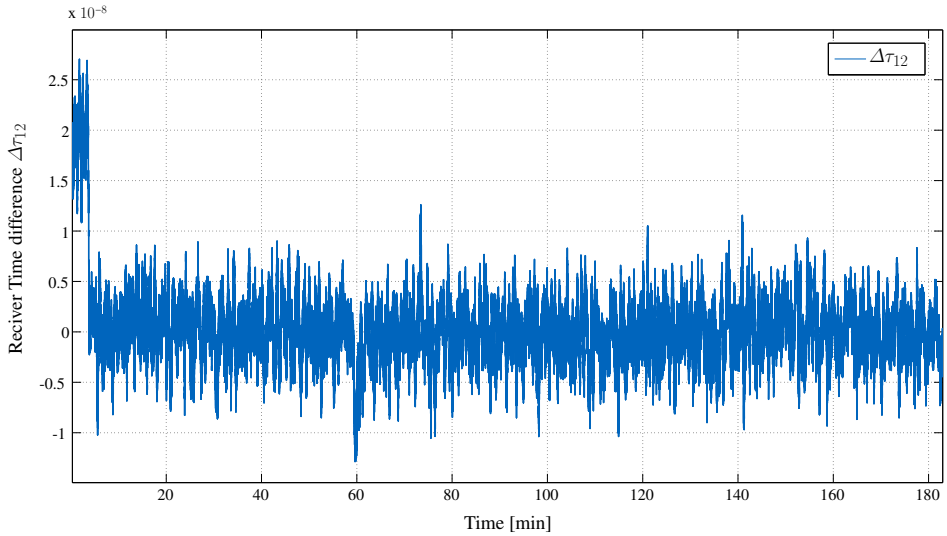

Figure 4.8: Receiver time offset difference $\Delta\delta\tau_{12}$ of two Novatel OEMStar™receivers with disabled clock steering.

As figure 4.5 and 4.6 the following figures show counter examples obtained by the Novatel OEMStar™receiver with disabled clock steering. One could easily see the clock drift. That explains the biases in the double difference measurements we show in figure 4.5 and 4.6. The clocks have been steered until at $t = 0$ the clock steering has been disabled and one could observe the following clock drift. Note that the axis is scaled with 10^{-4} this is an enormous drift which would make integer ambiguity impossible if no extra corrections were made for this effect.

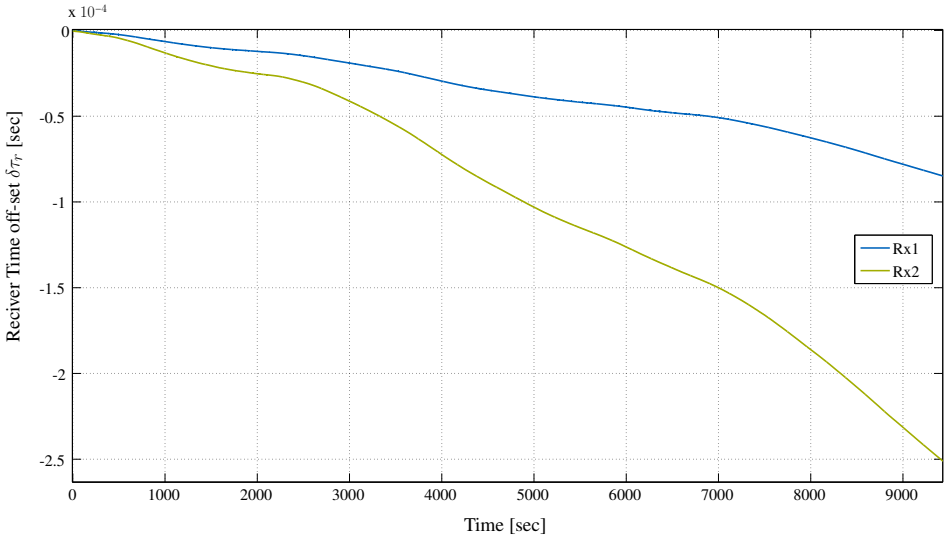

Figure 4.9: Receiver time offsets $\delta\tau_r$ of the Novatel OEMStar™receiver with disabled clock steering.

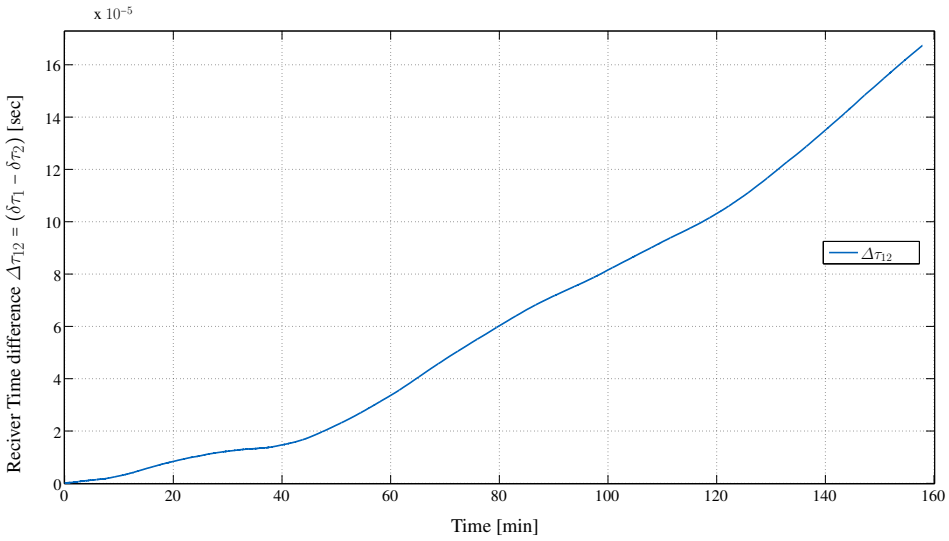

Figure 4.10: Receiver time offset difference $\Delta\delta\tau_{12}$ of two Novatel OEMStar™receivers with disabled clock steering.

4.3 Stationary Measurement

This section presents the results which are obtained from double difference measurements with a short baseline of 2m with the NovatelOEMStar™receiver. The first subsection explains the setup of the measurement and shows rough expectations for the heading and the baseline pitch angle. Then the second subsection shows the results of a fixed solution which is expected to be correct.

4.3.1 Measurement Setup

On top of the building of the Institute for Communication and Navigation at the Technical University of Munich we set up the antennas with two tripods. The two antennas are leveled so that the pitch angle is zero. The left figure shows the antennas before the measurement as they are leveled and aligned to a 2m baseline length. In the right figure the baseline orientation is shown with a red arrow and a rough expectation of the heading angle for plausibility checks is shown.

Figure 4.11: Stationary measurement setup of the top of the building of the Institute for Communication and Navigation at the Technical University of Munich.

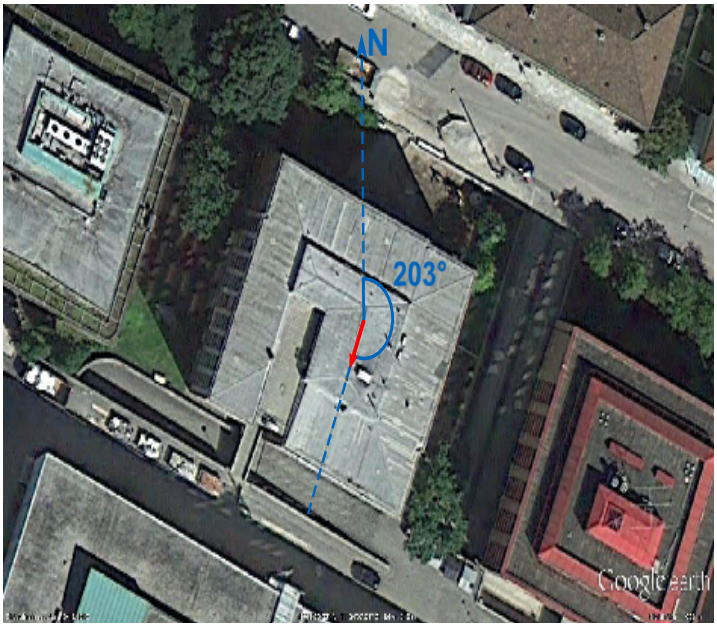

Figure 4.12: Top view to the building of the Institute for Communication and Navigation at the Technical University of Munich and the baseline denoted with a red arrow.

4.3.2 Measurement Results

The aim of this section is to show which accuracy could be achieved with correct integer fixing in a stationary environment. Therefore the integer search has been performed by the use of the Least Squares Ambiguity Decorrelation Adjustment (LAMBDA) method. The most likely correct integer is obtained by choosing from the set of baseline estimates, which fulfill the inequality constrained for the two meter baseline length, that one with the highest ratio. The ratio is defined as the squared error norm of the second best integer estimate over the squared error norm of the

best integer candidate.

$$R = \frac{\|\hat{\boldsymbol{\xi}} - \boldsymbol{\xi}_2\|^2}{\|\hat{\boldsymbol{\xi}} - \boldsymbol{\xi}_1\|^2} \tag{4.1}$$

Figure 4.13 shows the ratio over the baseline error. It is notable that during that measurement with 9 or 10 satellites available all the time the maximal baseline error is in the order of millimeter and the ratio has values up to 24.

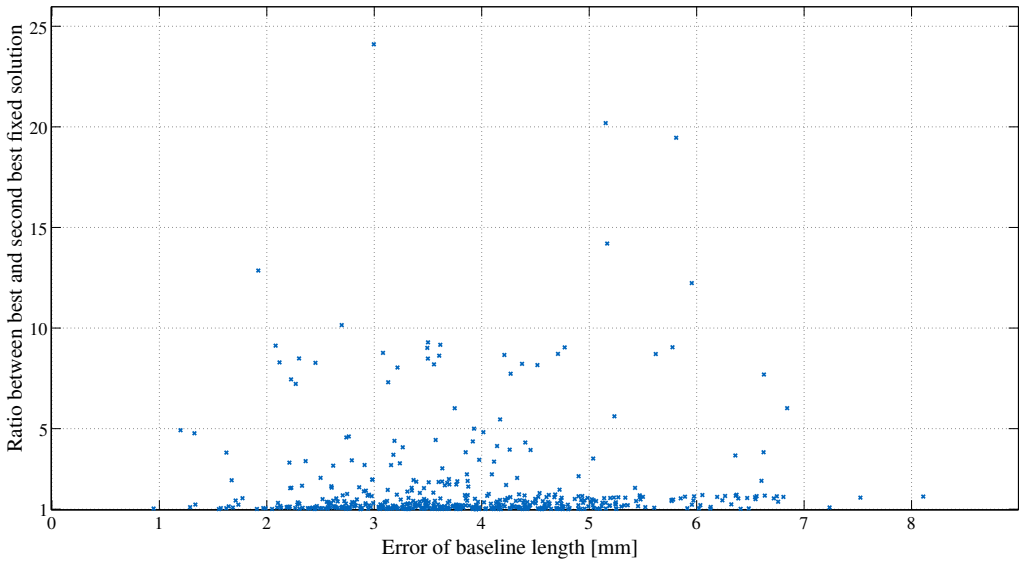

Figure 4.13: Value of the Ratio R plotted over the error of the baseline length obtained by the stationary measurement with a 2m baseline.

We chose the integer with the highest ratio and searched for further indications if we had made a right or wrong decision. Therefore the residuals give an indication if the solution has converged. The residuals are smaller than ±3cm no biases and major drift is visible. It is a good indication for a correct fixing.

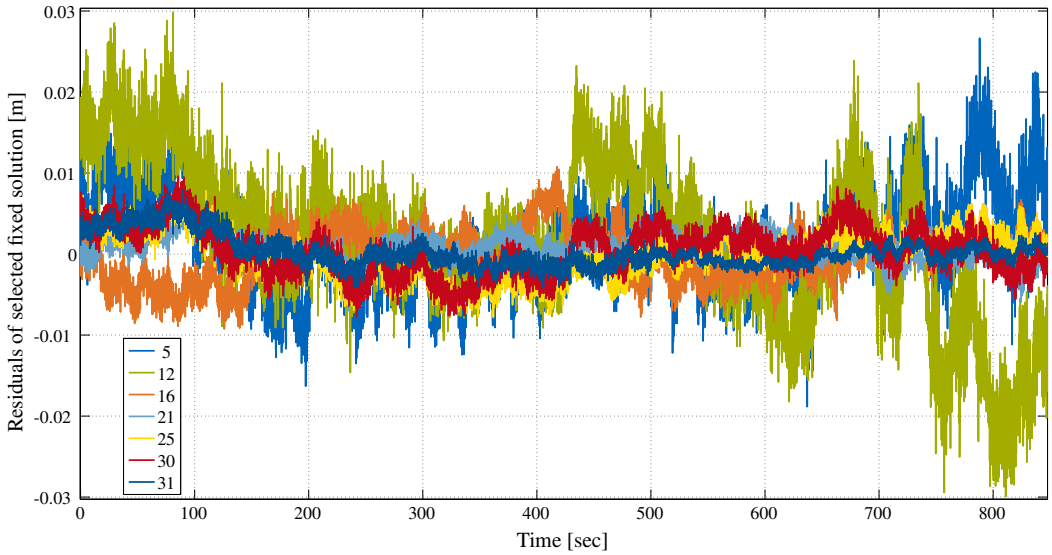

Figure 4.14: Residuals of the selected fixed solution as an indication for correct integer fixing.

We a adjusted the two antennas in a leveled way. For a correct fixing we expect the pitch angle of the estimated baseline to be zero. The figure below shows the estimated baseline pitch angle with variations of $\pm 0.6°$ around zero, it is a further indication that our fixing is correct.

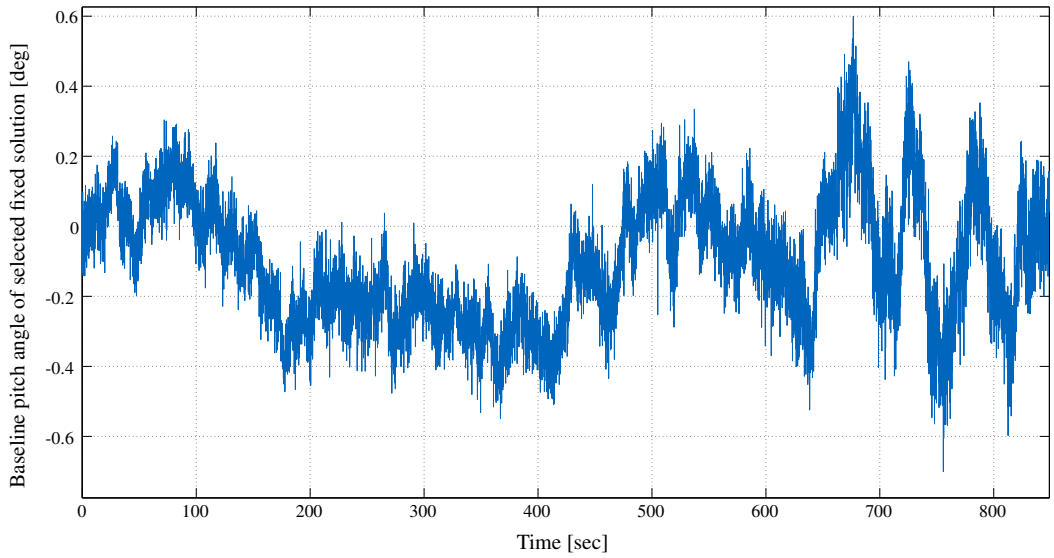

Figure 4.15: Baseline pitch angle of the selected fixed solution.

The same is true for the baseline length which is nominal 2m and with the estimate in figure 4.16 it is clear that the estimate is very likely to be the correct one. The variation around the mean value is roughly $\pm 6mm$. The mean value has a minimal offset which isn't that relevant because the accuracy how the true baseline length it determined with a yardstick isn't that accurate.

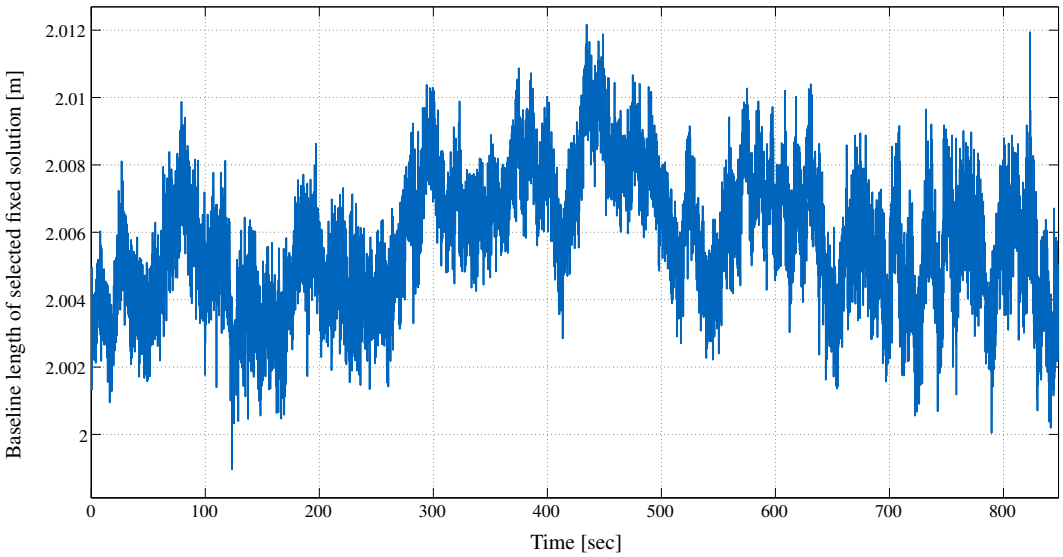

Figure 4.16: Baseline length of the selected fixed solution

Finally we obtain the heading of the selected fixed solution. Our rough estimate was $203°$ so the obtained value is feasible and with a noise level of $0.2°$ it is a very good result in respect to the baseline length. With a positioning accuracy in the order of roughly 7mm and a baseline of 2m that translates into a accuracy of the heading with $0.2°$. Compared to the pitch angle the heading angle is far more accurate, but this should be clear because the height component is every time not so accurate because of the overall geometry of a GNSS system.

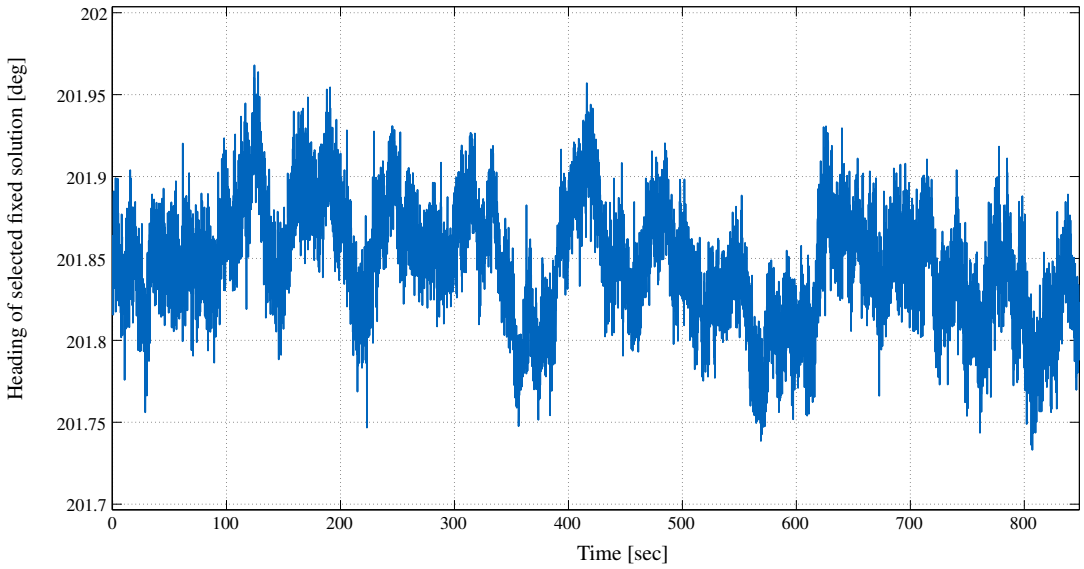

Figure 4.17: Heading of the selected fixed solution

4.4 Maritime Application

This section presents the results which are obtained from double difference measurements with a baseline of 20.65m with the NovatelOEMStar™receiver. The first subsection explains the setup of the measurement. Then the second subsection shows the results of a fixed solution which is expected to be correct.

4.4.1 Measurement Setup

The two antennas have been mounted at the front and back of an inland water vessel with a baseline of 20.65m. While the ship was traveling on the river under bridges and through a water gate, the measurements had been recorded. The pictures show the ship during the locking process.

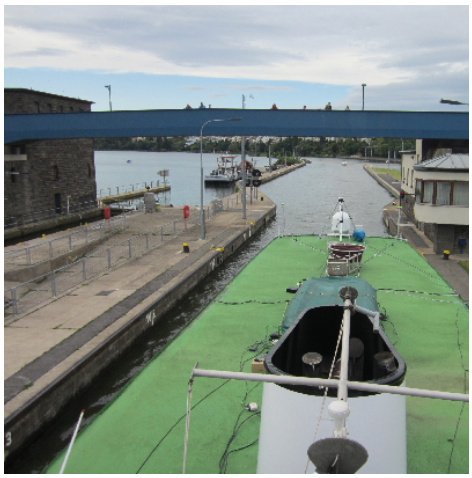

Figure 4.18: Rear view of the inland water vessel during the PiLoNav measurement campaign.

Figure 4.19: Front view of the inland water vessel during the PiLoNav measurement campaign.

4.4.2 Measurement Results

As in the section for the stationary measurments the aim of this section is to show which accuracy could be achieved with correct integer fixing in a maritime environment. Therefore the integer search has been performed by the use of the LAMBDA method. The most likely correct integer is obtained by choosing from the set of baseline estimates, which fulfill the inequality constrained for the baseline length, that one with the highest ratio. The ratio is defined as before; see (4.1). Figure 4.20 shows the ratio over the baseline error. In this dynamic case the errors are higher and and the ratio values are lower as expected. During that measurement up to 6 satellites have been visible. The concentration of the most baseline errors around $16\text{to}20mm$ is an indication that our estimate with the yardstick is probaly wrong by that amount

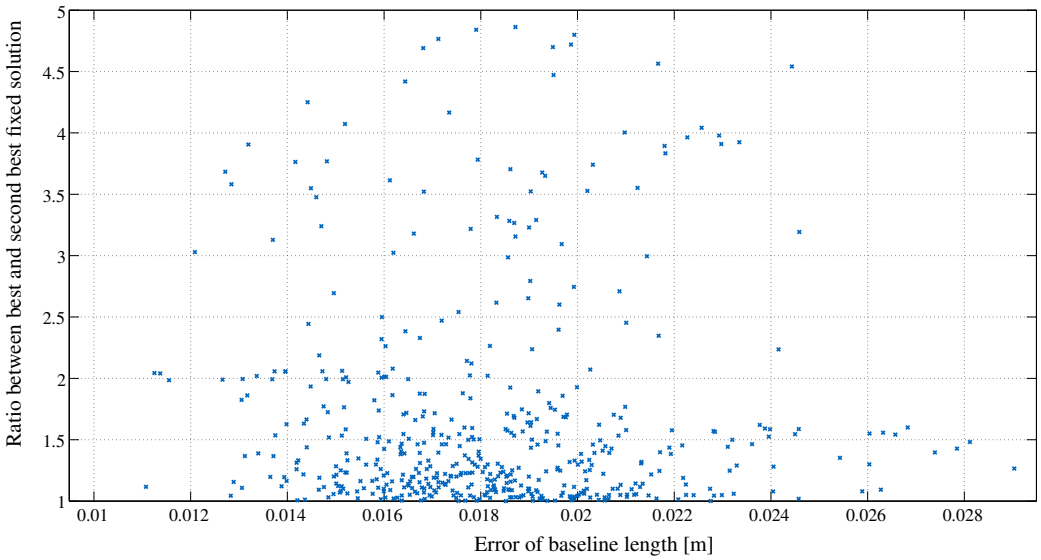

Figure 4.20: Ratio over the baseline error of all obtained estimates.

Again we chose the one with the highest ratio and try to verify if we have made a right or wrong decision. Figure 4.21 shows the residuals which are with maximal variations of $\pm 4cm$ nearly as good as in the stationary case.

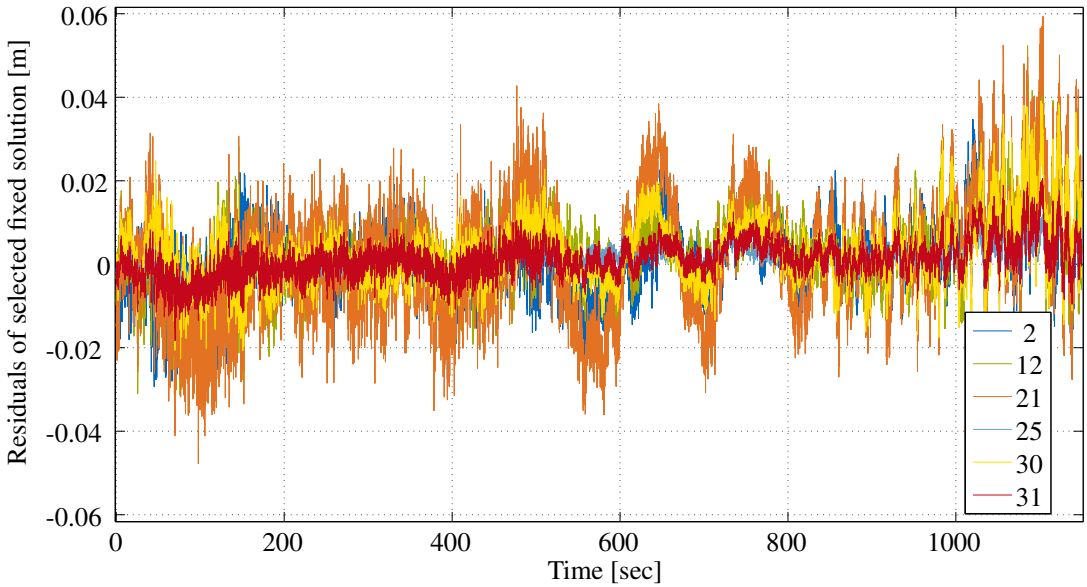

Figure 4.21: Residuals of the estimate of the selected fixed solution.

For the pitch angle we measured the height difference between the receivers over the deck of the ship with $0.77m \pm 0.15m$ additionally we have the uncertainty due to the fact that for this measurement we don't have more detailed information about the floating of the ship in the water. But the obtained estimate with variation around $2.5°$ is most likely to be correct.

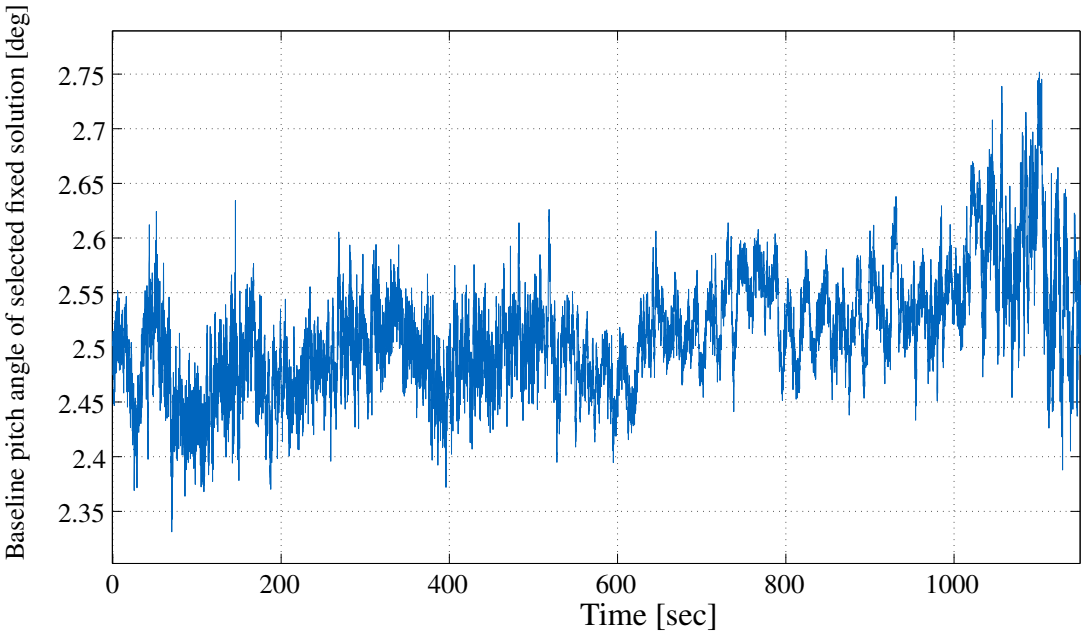

Figure 4.22: Baseline pitch angle estimate of the selected fixed solution.

A further look at the baseline length made us trust even more in the correctness of the obtained estimate. The small offset from the baseline estimate is in a reasonable size that it could be explained with the uncertainty with which the baseline length was determined.

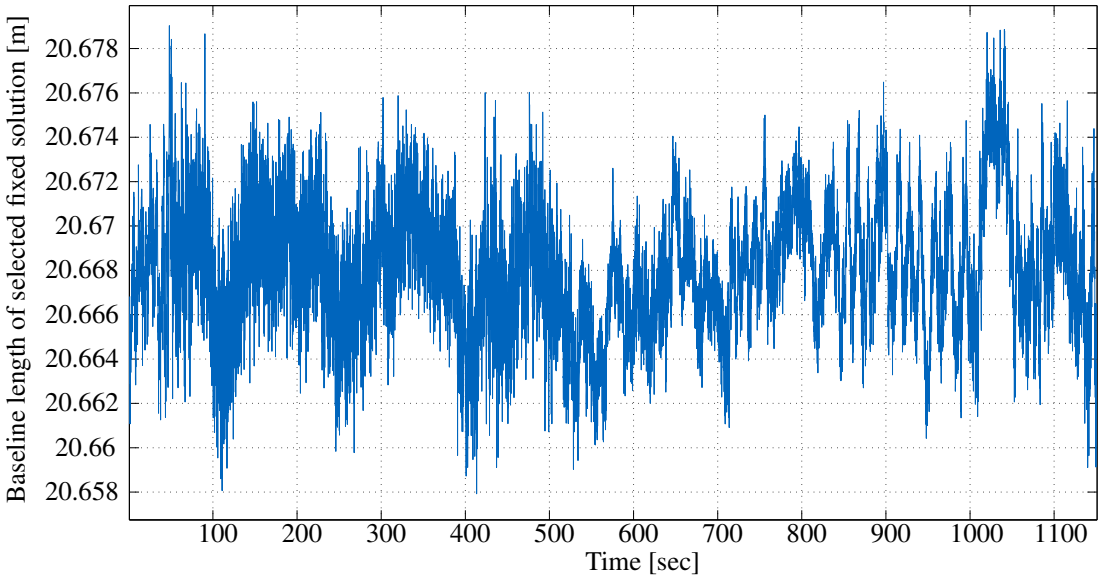

Figure 4.23: Baseline length estimate of the selected fixed solution.

The estimated heading is obtained without jumps during the measurement. To visualize the noise level figure 4.25 is a scaled version of the period from 605 to 630 seconds. There we see a noise level of $0.02°$ which we expected in the introduction.

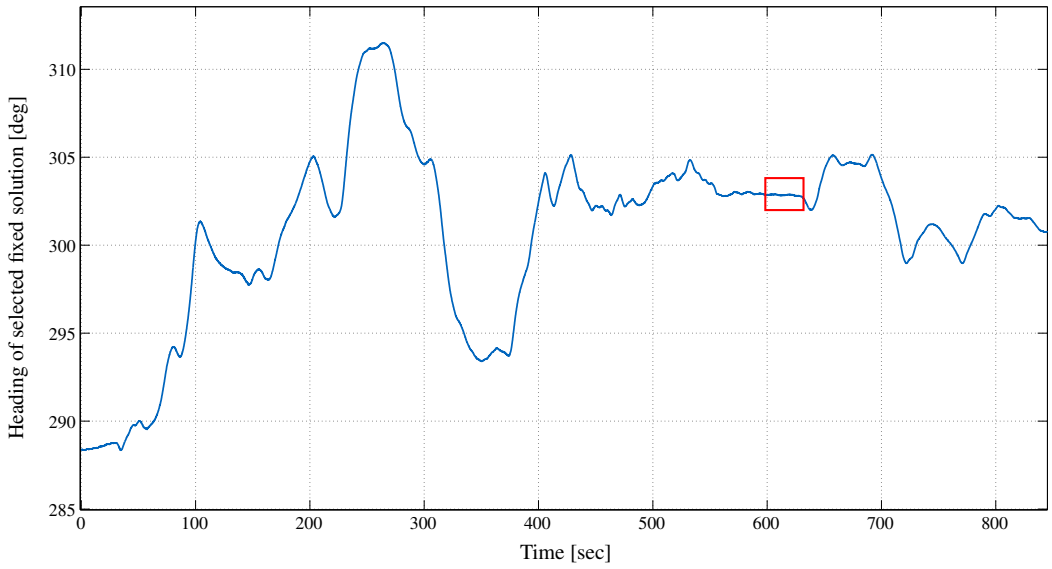

Figure 4.24: Heading of selected fixed solution.

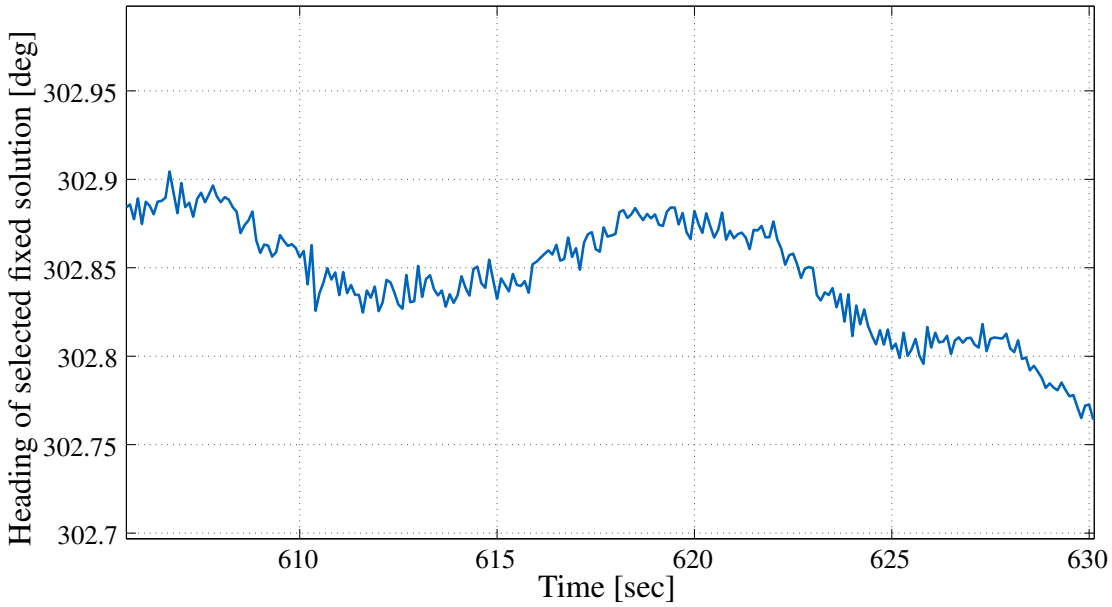

Figure 4.25: Heading of selected fixed solution scaled up to visulize the noise level.

As visualization of the estimated track and the heading at some epochs refer to the next figure. Figure 4.26 shows in green the track of the first receiver and in blue the heading of the baseline at different time instances.

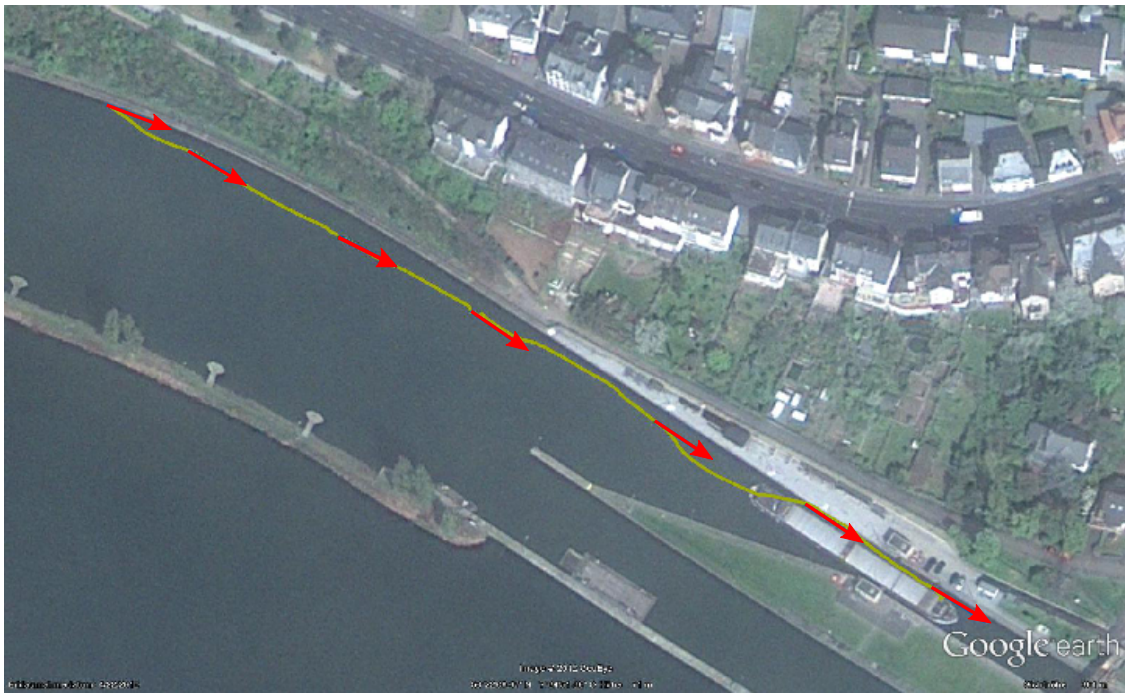

Figure 4.26: GPS track (green) of a ship during the PiLoNav measurement campaign on the river Mosel near Koblenz. The blue lines indicate the estimated heading at some epochs.

As a further interesting aspect obtained we would like to show the change in height during the locking process. It is obtained by the absolute position with a use of 60sec(600 epochs) carrier smoothing.

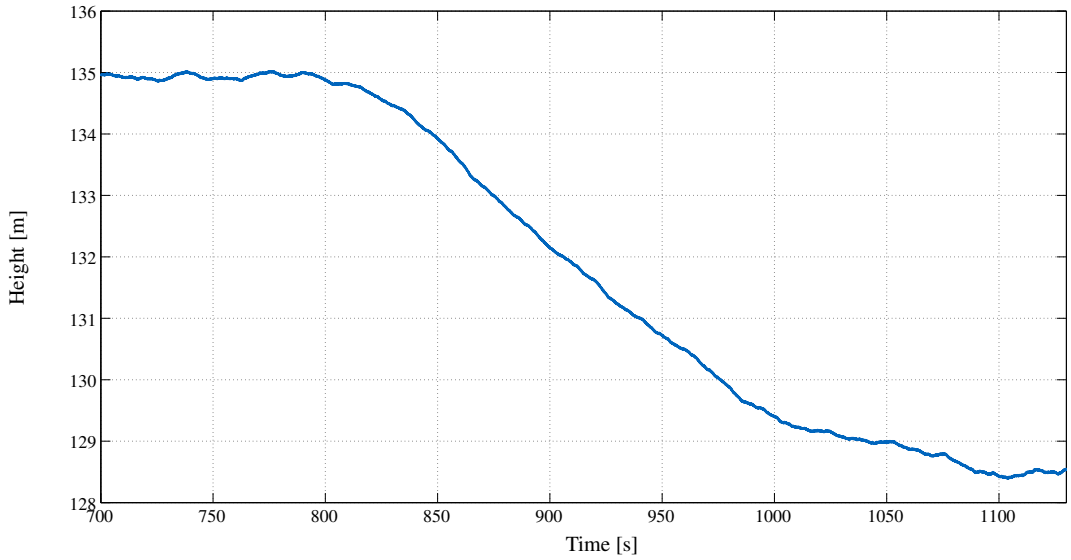

Figure 4.27: Change in height during the locking process of the ship.

5. Conclusion

Now we would like to sum up the work of this thesis. With the theoretical background of the carrier phase measurement the receiver quality has been analyzed. We found out that the NovatelOEMStar™receiver perfectly fulfills the requirements for double difference integer ambiguity resolution. If the clock steering is enabled, the receiver clock offsets are in the order of 10^{-8} or lower and the differential clock offsets between the two receivers are even smaller, due to the same clock steering loop. And the other requirements are fulfilled in the same way, resulting in constant integer values as seen in the zero baseline measurements. The analysis of the measurements in the stationary case as well as the measurements of the PiLoNav campaign on the river Mosel near Koblenz show very precise results after integer fixing. The residuals indicate a correct integer fixing because they are free of any biases and show no drift. Further the correct estimation of the baseline length and in addition to the stationary measurement the pitch angle indicates a very likely correct estimate for both cases. The obtained noise level of the estimated heading is in both cases in the order of $0.02°$. To conclude this, the mentioned receivers are perfectly suited for the application addressed in this thesis. But there are still some open questions which have to be considered. The implemented algorithm needs an initialization time to find an initial solution for the integer ambiguity. Further if many satellites are lost at the same time the reacquisition is hardly possible. To overcome this problem the idea of the improved soft constrained ambiguity resolution algorithm has been developed. There is the possibility that this improvement could make the algorithm applicable for single-epoch ambiguity resolution. But to show that, we propose to make simulations of the algorithm in the first step. After that, if the simulation results have been optimistic, in a second step the verification with experimental data could be done.

Appendix

A1. Cholesky Decomposition

The Cholesky Decomposition of a symmetrical and positive definite matrix $\boldsymbol{A}$ of dimention n is calculated in the following way:

$$\boldsymbol{A} = \boldsymbol{L}\boldsymbol{D}\boldsymbol{L}^T \tag{A1}$$

with the matrices shown in three dimensions:

$$\boldsymbol{L} = \begin{bmatrix} 1 & 0 & 0 \\ l_{21} & 1 & 0 \\ l_{31} & l_{32} & 1 \end{bmatrix} \tag{A2}$$

$$\boldsymbol{D} = \begin{bmatrix} d_{11} & 0 & 0 \\ 0 & d_{22} & 0 \\ 0 & 0 & d_{33} \end{bmatrix} \quad d_{kk} > 0 \tag{A3}$$

$$\boldsymbol{G} := \boldsymbol{L}\boldsymbol{D}^{\frac{1}{2}} \tag{A4}$$

$$\boldsymbol{A} = \boldsymbol{G}\boldsymbol{G}^T \tag{A5}$$

The calculation of $\boldsymbol{L}$ and $\boldsymbol{D}$ could be performed for the sequential columns $k = 1, 2, 3, ..., n$ with this explicit formulations:

$$d_{k,k} = a_{k,k} - \sum_{j=1}^{k-1} l_{i,j}^2 d_{j,j} \tag{A6}$$

$$l_{i,k} = \frac{1}{d_{k,k}}(a_{i,k} - \sum_{j=1}^{k-1} l_{i,j} d_{j,j} l_{k,j}) \tag{A7}$$

For reference and a more detailed explanation see [15].

A2. Chi-Squared Distribution

The Chi-Squared Distribution is defined as the sum of the squared n statistical independent and normal Gaussian distributed random variables X_i. The number n is understood as the degree of the chi-squared distribution.

$$\tilde{X} := \sum_{i=1}^{n} X_i^2 \qquad X_i \sim \mathcal{N}(0,1) \tag{A8}$$

The PDF of the chi-squared distribution is defined with the help of the Gamma function $\Gamma(z)$ as follows:

$$f_n(x) = \begin{cases} \dfrac{x^{\frac{n}{2}-1} e^{-\frac{x}{2}}}{2^{\frac{n}{2}} \Gamma(\frac{n}{2})}, & x \geq 0 \\ 0, & x < 0 \end{cases} \tag{A9}$$

$$\Gamma(z) := \int_0^\infty e^{-t} t^{z-1} dt \qquad z \in \mathbb{R}^+ \tag{A10}$$

In the following figure you can find the plots of the PDF for different values of n.

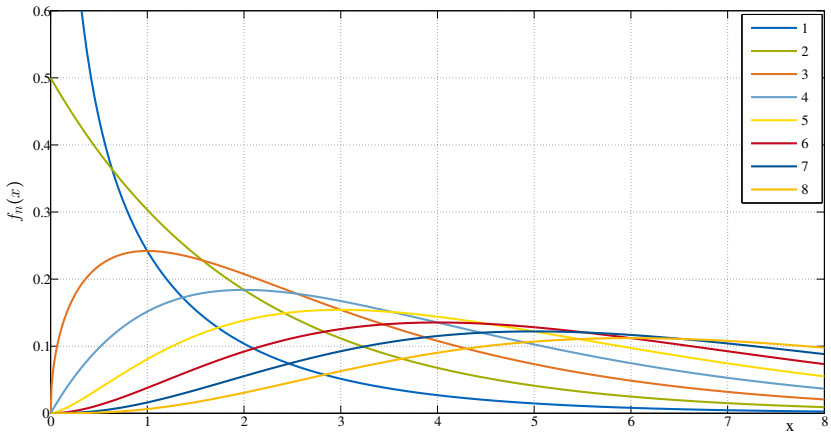

Figure A1: PDF of the χ_n^2 distribution with the dimension n.

Please note, in this thesis the dimension n is every time 3. Therefore the value of the $\Gamma(z)$ function is fixed. With $z = \frac{3}{2}$ we obtain $\Gamma(1.5) = 0.886227$. For further reference see [16].

A3. Acronyms

ADC	Analog Digital Converter
CDMA	Code Division Multiple Access
CDU	Control and Display Unit
COM	Communications Port
DC	Direct Current
DLL	Delay Locked Loop
ENU	East-North-Up Coordinate Frame
GLONASS	Globalnaja Nawigazionnaja Sputnikowaja Sistema
GNSS	Global Navigation Satellite System
GPS	Global Positioning System
IF	Intermediate Frequency
ILS	Integer Least Squares
LAMBDA	Least Squares Ambiguity Decorrelation Adjustment
LNA	Low Noise Amplifier
MAP	Maximum A Posteriori Probability
MATLAB	MATrix LABoratory
MC-LAMBDA	Multivariate Constrained - LAMBDA
ML	Maximum Likelihood
NCO	Numerical Controlled Oscillator
PDF	Probability Distribution Function
PiLoNav	Precise and integer Localisation and Navigation in Rail and Inlandwater Traffic
PLL	Phase Look Loop
RF	Radio Frequency
RINEX	Receiver Independent Exchange Format
USB	Universal Serial Bus

List of Figures

1.1 Two inland water vessels navigating close to each other on a water way. By Ikar.us (Karlsruhe:Bild:SchiffeMaxau.jpg) [CC-BY-2.0-de (http://creativecommons.org/licenses/by/2.0/de/deed.en)], via Wikimedia Commons 4
1.2 Integer Ambiguity 5
1.3 Classification of integer ambiguity resolution techniques. 5

2.1 Time scale definition 9
2.2 Propagation Model for Carrier Phase Measurement 10
2.3 Simple Model for Carrier Phase Measurement 11

3.1 Search tree: Constraints on the baseline length and orientation are checked at each path node to reduce the final number of branches. The tightness of the bounds and, thus the efficiency of the search, is determined by the prefactors μ_l,μ_{ν_1} and μ_{ν_2}[7].(Figure used with permission of Jurkowski P.) 24
3.2 PDF of the Chi-squared distribution with dimention three χ^2_3. 31
3.3 Search tree: Fulfillment of the constrains with a user defined failure rate are checked at each path node to reduce the final number of branches.(Figure adapted with permission of Jurkowski P.) 32

4.1 Novatel OEMStar Receiver with FlexPak G2 33
4.2 Novatel's CDU™software to either control the receiver and to log measurement data. 34
4.3 Double difference carrier phase measurements of a zero baseline test setup. It shows constant integer double difference values all the time the satellite is visible. 35
4.4 Double difference carrier phase measurements of a zero baseline test setup with respect to the rounded integer value of the 1st epoch a satellite is visible denoted as $[N_1]$. 36
4.5 Double difference carrier phase measurements of a zero baseline test setup with disabled clock steering. 37
4.6 Double difference carrier phase measurements of a zero baseline test setup with disabled clock steering and with respect to the rounded integer value of the 1st epoch a satellite is visible denoted as $[N_1]$. 37
4.7 Receiver time offsets $\delta\tau_r$ of the Novatel OEMStar™receiver with disabled clock steering. 38
4.8 Receiver time offset difference $\Delta\delta\tau_{12}$ of two Novatel OEMStar™receivers with disabled clock steering. 38
4.9 Receiver time offsets $\delta\tau_r$ of the Novatel OEMStar™receiver with disabled clock steering. 39
4.10 Receiver time offset difference $\Delta\delta\tau_{12}$ of two Novatel OEMStar™receivers with disabled clock steering. 39
4.11 Stationary measurement setup of the top of the building of the Institute for Communication and Navigation at the Technical University of Munich. 40

4.12 Top view to the building of the Institute for Communication and Navigation at the Technical University of Munich and the baseline denoted with a red arrow. 40
4.13 Value of the Ratio R plotted over the error of the baseline length obtained by the stationary measurement with a 2m baseline. 41
4.14 Residuals of the selected fixed solution as an indication for correct integer fixing. . 41
4.15 Baseline pitch angle of the selected fixed solution. 42
4.16 Baseline length of the selected fixed solution 42
4.17 Heading of the selected fixed solution 43
4.18 Rear view of the inland water vessel during the PiLoNav measurement campaign. 44
4.19 Front view of the inland water vessel during the PiLoNav measurement campaign. 44
4.20 Ratio over the baseline error of all obtained estimates. 45
4.21 Residuals of the estimate of the selected fixed solution. 45
4.22 Baseline pitch angle estimate of the selected fixed solution. 46
4.23 Baseline length estimate of the selected fixed solution. 46
4.24 Heading of selected fixed solution. 47
4.25 Heading of selected fixed solution scaled up to visulize the noise level. 47
4.26 GPS track (green) of a ship during the PiLoNav measurement campaign on the river Mosel near Koblenz. The blue lines indicate the estimated heading at some epochs. 48
4.27 Change in height during the locking process of the ship. 48

A1 PDF of the χ^2_n distribution with the dimension n. 51

Bibliography

[1] P. Henkel and C. Günther, "Reliable integer ambiguity resolution: Multi-frequency code carrier linear combinations and statistical a priori knowledge of attitude," *Navigation*, vol. 59, no. 1, pp. 61–75, 2012.

[2] P. J. Buist, "The baseline constrained lambda method for single epoch, single frequency attitude determination applications," *Proceedings of the 20th International Technical Meeting of the Satellite Division of The Institute of Navigation (ION GNSS 2007), Fort Worth, TX,*, pp. 2962–2973, 2007.

[3] S. Verhagen and P. J. G. Teunissen, "New global navigation satellite system ambiguity resolution method compared to existing approaches: Journal of guidance, control, and dynamics," *Journal of Guidance, Control, and Dynamics*, vol. 29, no. 4, pp. 981–991, 2006.

[4] P. J. G. Teunissen, "Least-squares estimation of the integer gps ambiguities," *Invited Lecture. Section IV Theory and Methodology, IAG General Meeting, Beijing, China*, 1993.

[5] G. Giorgi, P. J. Teunissen, S. Verhagen, and P. J. Buist, "Instantaneous ambiguity resolution in global-navigation-satellite-system-based attitude determination applications: A multivariate constrained approach," *Journal of Guidance, Control, and Dynamics*, vol. 35, no. 1, pp. 51–67, 2012.

[6] P. Jurkowski, "Baseline constrained ambiguity resolution with multiple frequencies: Bachelor thesis," 2010.

[7] P. Jurkowski, P. Henkel, G. X. Gao, and C. Günther, "Integer ambiguity resolution with tight and soft baseline constraints for freight stabilization at helicopters and cranes," *Proceedings of the Intern. Techn. Meeting of the Inst. of Navigation (ION-ITM),San Diego, USA*, 2011.

[8] A. Kleusberg and P. J. G. Teunissen, *GPS for geodesy*. Berlin and and New York: Springer, 2 ed., 1998.

[9] B. W. Parkinson and J. J. Spilker Jr., *Global Positioning System: Theory and Applications Vol. I*, vol. 163 of *Progress in Astronautics and Aeronautics*. Washington and D.C: American Inst. of Aeronautics and Astronautics, 7 ed., (1996).

[10] P. Misra and P. Enge, *Global positioning system: Signals, Measurements, and Performance*. Lincoln and Massachusetts: Ganga-Jamuna Press, 2 ed., 2006.

[11] C. O'Driscoll, "Gnss solutions: Carrier phase and its measurment for gnss: What is the carrier phase measurement? how is it generated in gnss receivers?," *Inside GNSS*, vol. 5, no. 5, pp. 18–22, 2010.

[12] M. L. Psiaki and S. Mohiuddin, "Modeling, analysis, and simulation of gps carrier phase for spacecraft relative navigation," *Journal of Guidance, Control, and Dynamics*, vol. 30, no. 6, pp. 1628–1639, 2007.

[13] P. Henkel and P. Jurkowski, "European patent application: Method and apparatus for determining the relative position between two receivers of a satellite navigation system, ep2479588," 2012.

[14] NovAtel Inc., "Oemstartm installation and operation user manual," 2011.

[15] W. Dahmen and A. Reusken, *Numerik für Ingenieure und Naturwissenschaftler*. Berlin and Heidelberg: Springer, 2 ed., 2006.

[16] L. Råde, B. Westergren, and P. Vachenauer, *Springers mathematische Formeln: Taschenbuch für Ingenieure, Naturwissenschaftler, Informatiker, Wirtschaftswissenschaftler*. Berlin and Heidelberg: Springer, 3 ed., 2000.